Discrete element simulation for the evaluation of solid mixing in an industrial blender

Mikio Sakai[a*], Yusuke Shigeto[b], Gytis Basinskas[c], Akira Hosokawa[d], Masayoshi Fuji[e]

a *Resilience Engineering Research Center, School of Engineering, The University of Tokyo*
7-3-1 Hongo, Bunkyo-ku, Tokyo 113-8656, Japan
Tel: +81-3-5841-6977; Fax: +81-3-5841-6977
E-mail: mikio_sakai@n.t.u-tokyo.ac.jp
Corresponding author

b *Department of Systems Innovation, School of Engineering, The University of Tokyo*
7-3-1 Hongo, Bunkyo-ku, Tokyo 113-8656, Japan

c *Department of Nuclear Engineering and Management, School of Engineering*
The University of Tokyo, 7-3-1 Hongo, Bunkyo-ku, Tokyo 113-8656, Japan

d *Department of Systems Innovation, Faculty of Engineering, The University of Tokyo*
7-3-1 Hongo, Bunkyo-ku, Tokyo 113-8656, Japan

e *Advanced Ceramic Research Center, Nagoya Institute of Technology*
3-101-1 Hon-machi, Tajimi, Gifu 507-0033, Japan

Abstract

Recent improvements in computer hardware have made it possible to simulate granular flow in an industrial system. There is a desire in industry to apply a numerical technology to design of an actual powder process. In the present study, the discrete element method (DEM) was applied to a twin-screw kneader as an example of an actual industrial blender, and the mixing efficiency was investigated for different operational parameters. The complexly shaped wall boundaries of the paddles and vessel were created using the signed distance function (SDF). Validation tests were first performed to demonstrate the applicability of the DEM employing the SDF-based wall boundary model. In the validation tests, simulations and experiments were shown to be in quantitative agreement in terms of the spatial distribution of solid particles. The mixing efficiency was then investigated for different rotational speeds and amounts of powder, where the degree of mixing was evaluated using Lacey's mixing index. The numerical simulation could clarify the mixing mechanism behind observed phenomena. The study thus illustrated that the total amount of powder affected the mixing efficiency of the twin-screw kneader.

Keywords: discrete element method, signed distance function, twin-screw kneader, degree of mixing

1. Introduction

Industry manufactures many products employing powder-mixing processes. The powder is often agitated in blenders having complex shapes [1][2], such as a twin-screw kneader and a ribbon mixer. In an experimental study, the degree of mixing [3] is often evaluated using marker particles, where it is assessed by sampling the colored particles, e.g., reference [4][5]. Evaluation of the mixing degree might not be accurate because the physical properties might differ between types of marker particles owing to different material or surface properties and because sampling might change the particle location when the powder is scooped up. Besides, scale of scrutiny might influence the evaluation of the degree of mixing. Hence, experimental studies on the degree of mixing might face some problems from the viewpoint of accuracy. To solve the problem, numerical simulation is desired to be applied to the evolution of the degree of solid mixing. The numerical simulation can set ideally the physical properties of all particles, although the particles are colored differently. Effect of scale of scrutiny on the degree of mixing can also be investigated by the computer simulation. Additionally, the particle location is unaffected when numerical simulation is employed to evaluate the mixture state.

The discrete element method (DEM) [6] is often employed as a numerical method for granular flow. The DEM is a Lagrangian approach, where individual particle

motion is computed according to the Newton's second law of motion. In the usual DEM simulations, the contact force acting on a particle is simply modeled using springs, dashpots and a friction slider. When more accurate contact modeling is required, sophisticated models such as a non-linear spring model [4][7] can be employed. The DEM has been applied to various industrial powder processes, such as those of a screw conveyer [8] and a mill [9]. The DEM can also be applied to simulate complex phenomena related to agglomeration due to cohesive forces [10], segregation in a poly-dispersive system [11] and the behavior of non-spherical particles [12][13]. Recently, the DEM has been applied to complex systems such as those in which there are solid–fluid interactions. In these applications, the behavior of solid particles can be simulated by coupling the DEM with computational fluid dynamics (CFD). This methodology is referred to as the DEM–CFD method [14]. The DEM–CFD method has been used to model a variety of dense gas–solid flows such as a bubbling fluidized bed [15][16][17][18][19] and pneumatic conveying [20][21]. Very recently, new Lagrangian–Lagrangian approaches have been developed to simulate solid–liquid flows involving free surfaces, where the DEM is coupled with a Lagrangian CFD approach such as the smoothed particle hydrodynamics (SPH) method [22] or the moving-particle semi-implicit (MPS) method [23]. The Lagrangian–Lagrangian approach is thus

referred to as the DEM–MPS method [24][25][26] or the DEM–SPH method [27]. These methods can be used to simulate complex solid–fluid coupling problems such as those of wet ball mills. Hence, the DEM is regarded a reliable approach for the simulation of a complex granular flow. On the other hand, the DEM has been applied to simple domains such as rectangular, circular, cuboid, cylindrical and conic domains in previous studies. However, the DEM has rarely been applied to complexly shaped devices in industrial systems.

A proper understanding of granular flow employing numerical simulation is important in optimizing the device design or operational conditions in industry. When the DEM simulation is performed for an industrial blender, the complex shape boundary must be modeled precisely. In previous studies [28][29], meshes were employed to create the wall boundary of the complexly shaped device. The meshes have commonly been used in simulations employing the finite element method and finite volume method. When the meshes are applied in a DEM simulation, complex and difficult procedures are needed to program particle-to-wall collisions; i.e., several procedures are carried out for collision detection between a solid particle and mesh components such as the node, edge and surface. Therefore, the mesh-based boundary has not been employed in in-house software developed at universities and institutes. Hence, it is not always

possible for researchers to model the complex wall boundary when the granular flow simulation is performed for a system having a complexly shaped boundary. On the other hand, very recently, the authors developed a new wall boundary model, which is called the signed distance function (SDF) [30], to solve the problem of the complexly shaped boundary of the DEM. The SDF makes it possible to perform a DEM simulation without requiring a complex procedure in programming the particle-to-wall interaction. A previous study [30] verified the application of the SDF model to the DEM simulation of industrial systems such as a screw conveyer and a mill. We refer to the DEM employing the SDF-based wall boundary model as the DEM/SDF. The DEM/SDF is a promising approach for the simulation of granular flow in a complexly shaped blender. However, the DEM/SDF has not been validated thus far, though its adequacy has been verified. Additionally, the DEM/SDF has not been applied to a practical problem such as the evaluation of the mixing degree of a powder mixture.

In this study, the DEM/SDF is applied to solid mixing in an actual industrial problem. This study investigates which operational parameters of a twin-screw kneader or blender (in this paper, this system is simply called the twin-screw kneader), where mono-dispersed powders are mixed in two rooms by complexly shaped paddles, affect the solid mixing efficiency. Indeed, this system is used for mixing in chemical

engineering [31][32], pharmaceutics [33][34], etc. The DEM/SDF has not previously been applied to a twin-screw kneader. Hence, validation tests are first performed to show the agreement between the results of the DEM/SDF simulation and experiment for the kneader. The mixing degree is then evaluated by changing operational parameters such as the rotational speed of the paddles and the amount of powder. Indeed, the degree of mixing is shown for the first time to be affected by not only the rotational speed, but also the amount of powder. Furthermore, it is newly illustrated that the degree of mixing becomes high when the powder is well moved from one room to the other one. Consequently, adequacy of the DEM/SDF is validated and mixing mechanism is clarified in the twin-screw kneader through this study.

2. Numerical modeling

2.1 Motion of solid particles

Modeling of the motion of solid particles is first briefly described. In the DEM, the motion of individual particles is modeled according to the Newton's second law of motion. The translational and rotational motions of a solid particle are respectively expressed by

$$m\boldsymbol{a} = \sum \boldsymbol{F}_C + \boldsymbol{F}_g \tag{1}$$

and

$$\frac{d}{dt} = \frac{\sum \boldsymbol{T}}{I}, \tag{2}$$

where m, $\boldsymbol{a}$, $\boldsymbol{F}_C$, $\boldsymbol{F}_g$, $\boldsymbol{\omega}$, $\boldsymbol{T}$ and I are the mass, acceleration, contact force, gravitational force, angular velocity, torque and moment of inertia of a solid particle, respectively. $\boldsymbol{F}_C$ can be divided into normal and tangential components as

$$\boldsymbol{F}_C = \boldsymbol{F}_{C_n} + \boldsymbol{F}_{C_t}, \tag{3}$$

where the subscripts n and t indicate normal and tangential components. The contact force acting on a solid particle is the sum of elastic and damping forces. The elastic force is expressed on the basis of the Hooke's law. The normal component of the contact force is given by

$$\boldsymbol{F}_{C_n} = -k\boldsymbol{\delta}_n - \eta \boldsymbol{v}_n, \tag{4}$$

where k, $\boldsymbol{\delta}$, $\boldsymbol{v}$ and η are the spring constant, displacement, relative velocity of a solid particle and damping coefficient, respectively. η is given as

$$\eta = 2 \ln e \sqrt{\frac{m\,k}{(\ln e)^2 + \pi^2}}, \tag{5}$$

where e is the coefficient of restitution.

The tangential component of the contact force is

$$\boldsymbol{F}_{C_t} = \begin{cases} -k\boldsymbol{\delta}_t - \eta \boldsymbol{v}_t & \left(\left|\boldsymbol{F}_{C_t}\right| \le \mu \left|\boldsymbol{F}_{C_n}\right|\right) \\ -\mu \left|\boldsymbol{F}_{C_n}\right| \boldsymbol{t} & \left(\left|\boldsymbol{F}_{C_t}\right| > \mu \left|\boldsymbol{F}_{C_n}\right|\right) \end{cases}, \tag{6}$$

where μ and $\boldsymbol{t}$ are the friction coefficient and tangential vector, respectively.

2.2 Wall boundary model based on the SDF

Our previous study proposed a new wall boundary model based on SDF that allows a DEM simulation to be performed in an arbitrarily shaped domain with a simple algorithm. The SDF model greatly simplifies the computation of the interaction between the particle and wall in comparison with that of the existing wall boundary model. Additionally, the SDF model has the advantage that energy is conserved in a non-dissipative system. In other words, energy dissipation can be simulated precisely. Details of the DEM/SDF are described in the literature [30]. The SDF model is briefly explained in the present paper.

In the SDF model, the wall boundary is represented by the zero-level contour. The SDF ϕ is defined as

$$\phi(\boldsymbol{x}) = d(\boldsymbol{x}) \cdot s(\boldsymbol{x}), \tag{7}$$

where $d(\boldsymbol{x})$ is the minimal distance from the point $\boldsymbol{x}$ to the surface of the wall and $s(\boldsymbol{x})$ is the sign, which is negative/positive for $\boldsymbol{x}$ inside/outside the calculation domain. The

normal vector $\boldsymbol{n}$ at the boundary is defined as

$$\boldsymbol{n} = \frac{\nabla \phi}{|\nabla \phi|}. \tag{8}$$

When a solid particle makes contact with the wall, the normal component of displacement $\boldsymbol{\delta}_n^{SDF}$ is obtained as

$$\boldsymbol{\delta}_n^{SDF} = (\phi - r) \cdot \boldsymbol{n}, \tag{9}$$

where r is the radius of the solid particle. The normal component of the contact force is given by

$$\boldsymbol{F}_{C_n}^{SDF} = -k\boldsymbol{\delta}_n^{SDF} |\nabla \phi| - \eta \boldsymbol{v}_n. \tag{10}$$

Energy is conserved in non-dissipative systems because of the term $|\nabla \phi|$ in eq. (10). The energy dissipation due to the damper was modeled by the same manner as that of the existing DEM. The energy conservation results from the elastic force being the gradient of energy:

$$\begin{aligned} \boldsymbol{F} &= \nabla P \\ &= -k(r - \phi) \cdot \nabla \phi, \\ &= -k\boldsymbol{\delta}^{SDF} \cdot |\nabla \phi| \end{aligned} \tag{11}$$

where $\boldsymbol{F}$ and P are, respectively, elastic force and the potential energy; i.e., elastic energy. Hence, the tangential component of the contact force is obtained in the same manner as that of the existing boundary model. The tangential component of the contact force is given by

$$\boldsymbol{F}_{C_t} = \begin{cases} -k\boldsymbol{\delta}_t^{SDF} - \eta \boldsymbol{v}_t & \left(\left|\boldsymbol{F}_{c_t}\right| \le \mu \left|\boldsymbol{F}_{C_n}\right|\right) \\ -\mu\left|\boldsymbol{F}_{C_n}\right| \dfrac{\boldsymbol{v}_t}{\left|\boldsymbol{v}_t\right|} & \left(\left|\boldsymbol{F}_{c_t}\right| > \mu\left|\boldsymbol{F}_{C_n}\right|\right) \end{cases}, \tag{12}$$

where $\boldsymbol{\delta}_t^{SDF}$ is the tangential component of displacement and is obtained in the same manner as when using the existing DEM.

3. Mixing index

Lacey's mixing index M (Lacey, 1954) [35], which has been widely employed for various mixers [36] [37], is used to evaluate the degree of mixing and is expressed as

$$M = \frac{\sigma_0^2 - \sigma_t^2}{\sigma_0^2 - \sigma_r^2}, \tag{13}$$

where σ_t^2, σ_0^2 and σ_r^2 are the variance based on the current particle location, the variance in a completely segregated system and the variance in a perfectly mixed system, respectively. σ_t^2, σ_0^2 and σ_r^2 are given by

$$\sigma_t^2 = \frac{1}{p-1}\sum_{i=1}^{p}\left(c_i - c_m\right)^2, \tag{14}$$

$$\sigma_0^2 = c_m\left(1 - c_m\right), \tag{15}$$

$$\sigma_r^2 = \frac{c_m\left(1 - c_m\right)}{q}, \tag{16}$$

where p is total number of sampling cells from this system, c_i is the local concentration in a sampling cell, c_m is the overall proportion of one type of particle in the system, and

q is the average particle number over all sampling cells.

Number of sampling cells or cell size might influence estimation of the degree of mixing. In previous study [7], sensitive analyses were performed by changing the number of the cells in a slant cone mixer. This study showed that degree of mixing was not affected remarkably by the resolution. Besides, small number of calculated particles in the cell makes the valiance inaccurate [4]. These studies imply that reliable values of mixing degree could be obtained when the average number of calculated particles in the cell should be 30 to 200.

4. Validation tests

4.1 Validation conditions

Validation tests were performed to show the agreement between the DEM simulations and actual phenomena in a twin-screw kneader. In this study, mixing process of dry powder was focused. Simulation and experimental results were compared for the apparent solid particle location and particle bed height. Figure 1 is a schematic diagram of the experimental device used in the validation tests. The height, width and length were respectively 106, 186 and 46 mm. The clearance between the paddle edge and the interior of the vessel wall was 3.0 mm. Four paddles were equipped in the depth

direction. In the actual kneading processes, this configuration is continued periodically. The paddles were rotated in a clockwise direction, and the rotational velocity of the paddle Ω was 20 and 60 rpm in the validation tests. Table 1 gives the physical properties. Glass beads having an average diameter of approximately 1.0 mm were used in the tests. The total amount of powder was set to 0.262 kg and 0.524 kg, respectively. The particle behavior was recorded by a high-speed camera (Vision Research Phantom V9.1).

Calculation conditions were set to compare the simulation and experimental results fairly. Mono-sized particles with diameter of 1.0 mm were used in the calculations. Simple linear contact model was used in this study. The spring constant, coefficient of friction and coefficient of restitution were set as 1000 N/m, 0.3 and 0.9, respectively. These values of physical properties were commonly used in the previous DEM simulations. Table 2 gives the calculation conditions. The number of particles N in the calculation was 200,000 in Case 1-1 and 400,000 in Case 1-2, where the weight corresponded to that in the experiment. The time step was set to 1.0×10^{-5} s and the number of iterations was set to 1.6×10^{6}. The wall boundary was modeled by the SDF. Figure 2 shows the SDF for four cross-sectional views of the paddle. In the figure, blue and red regions are respectively regions inside and outside the paddle. The distance and sign were given for the whole computational domain; i.e., the two paddles and the

vessel.

Not only adequacy of the DEM/SDF but also applicability of the linear contact model and the physical properties is proved through the validation tests.

4.2 Validation results

Figures 3 and 4 show the validation test results in Case 1-1 and Case 1-2, respectively. It is seen that the simulation and experiment were in qualitative agreement in terms of the spatial distribution of particles; specifically, particles were located much more on the left side. The bed height was quantitatively compared between the simulations and experiments. The bed height was respectively 87.40 and 88.76 mm in the simulation and experiment in Case 1-1. In Case 1-2, the bed height was estimated to be 101.81 and 101.24 mm respectively in the simulation and experiment. The differences between the simulation and experiment were thus extremely slight; i.e., the simulation errors were estimated to be less than 0.6%.

The validation test results thus indicate that the DEM/SDF simulates the particle location precisely. This implies that the DEM/SDF can be applied to an actual problem such as the degree of mixing in a blender. Besides, applicability of the linear contact model and the above physical properties is shown in this kneader.

5. Numerical evaluation of the mixing degree

The effects of the rotational speed and amount of powder on the mixing efficiency, namely, mixing degree per unit time, were numerically investigated for nine combinations of conditions in the twin-screw kneader. This system is classified into a convective mixer, where the main mechanism is generally regarded to be convective mixing, and diffusive and shear mixing are also accompanied. Detailed mixing mechanism is investigated in this study.

5.1 Calculation conditions

The configuration and physical properties were the same as those in the validation tests and presented in Fig. 1 and Table 1. Table 3 denotes the calculation conditions. In this study, the parameters were the number of particles and rotational speed of the paddles. The number of particles was set as 100,000, 200,000 and 400,000, while the rotational speed was set as 15, 30 and 60 rpm. Black and white particles with equivalent physical properties were used to evaluate the degree of mixing. To compare the mixing efficiency fairly, all the calculations were finished when the physical time became 16 s.

In evaluating the degree of mixing, number of sampling cells was decided by the sensitive analyses. The degree of mixing was compared by the calculation results, where the number of sampling cells was 6,993 (21 x 37 x 9 in the vertical, horizontal and depth direction) and 1,155 (11 x 21 x 5 in the vertical, horizontal and depth direction). Although detailed comparison was not shown in this paper, both results approximately agreed regardless of the different cell number. In this study, the number of cells was decided to be 6,993 (cell size was around 5 mm) for the evaluation of mixing degree, where the average number of particles in the cell was around 110.

5.2 Results and discussion

(1) Effect of the rotational speed on the degree of mixing

The degree of mixing was first investigated for the three rotational speeds and 100,000 particles (Case 2). Figure 5 shows typical snapshots obtained in the simulation. Many more particles were located in the left room than in the right room. The black and white particles were mixed by the paddle rotation. When the rotational speed reached 60 rpm, scattered particles were observed. Figure 6 presents the transient change in the degree of mixing. The degree of mixing increased with the rotational speed. The degree of mixing corresponded to the observed particle distribution. To comprehend the mixing

mechanism behind observed phenomena, degree of mixing per rotation was evaluated in this study. Snapshots of the degree of mixing per rotation are presented in Fig. 7. In Case 2-1, there is no calculation result after the fourth rotation because the calculation was complete after four rotations. Although the binary mixture proceeded slowly in Cases 2-1 and 2-2, it preceded much more in Case 2-3 because of the scattered particles. Figure 8 presents the relation between the degree of mixing and rotation. The mixing efficiency at 60 rpm was better than that at 30 rpm. This is because the movement of many scattered particles from the left room to the right room was observed at only 60 rpm as shown in Fig. 9. Hence, there was a much more exchange of particles between the left and right rooms only at 60 rpm, and the degree of mixing was thus enhanced by the scattered particles.

Then, in Case 3, the degree of mixing was evaluated when the vessel was filled with powder to around half height. Figure 10 shows the simulation results. In the same way as Case 2, many more particles were located in the left room than in the right room. The black and white particles were mixed by the paddle rotation. Scattered particles were observed when the rotational speed reached 60 rpm. Figure 11 presents the transient change in the degree of mixing for 200,000 particles. The degree of mixing increased with the rotational speed. Degree of mixing per rotation was evaluated to

understand the mixing mechanism. Representative snapshots of the degree of mixing per rotation are shown in Fig 12. In Cases 3-1 to 3-3, the locations of black and white particles except for the scattered particles were similar, regardless of the paddle speed. Figure 13 presents the relation between the degree of mixing and rotation. The degree of mixing was approximately the same regardless of the rotational speed in Cases 3-1 to 3-3. This result implies that the degree of mixing per number of rotations was hardly affected by the rotational speed. In Cases 3-1 to 3-3, as shown in Fig. 14, avalanches were observed near the boundary of the two rooms, and there was thus a much more exchange of particles between the left and right rooms.

Finally, the effect of the mixing degree on rotational speed was investigated for a large quantity of particles (i.e., 400,000 particles, Case 4) in the kneader. Figure 15 shows the simulation results. Slightly more particles were located in the left room than in the right room. The black and white particles mixed gradually. Scattered particles were hardly observed in Case 4. Figure 16 presents the transient change in the degree of mixing. The degree of mixing increased with the rotational speed as in Cases 2 and 3. Degree of mixing per rotation was calculated to figure out the mixing mechanism. Typical snapshots of the degree of mixing per number of rotations are shown in Fig. 17. Distributions of black and white particles were similar regardless of the rotational speed.

Figure 18 presents the relation between the degree of mixing and rotation. The degree of mixing did not depend on the rotational speed in Cases 4-1 to 4-3. This result implies that the degree of mixing per number of rotations was hardly affected by the rotational speed in Case 4. As shown in Fig. 19, in Cases 4-1 to 4-3, there were avalanches in the right room, and the mixing efficiency was thus only affected by the exchange of particles at the boundary of the two rooms.

(2) Effect of the amount of powder on the mixing degree

Figures 20 to 22 show the effect of the amount of powder on the degree of mixing. In all figures, the mixing efficiency was optimal when the number of particles was 200,000. This is because there was a much more exchange of solid particles from left to right room when the number of particles was 200,000 as shown in Fig. 14. Specifically, when the vessel was filled with powder to around half height, the avalanches occurred near the boundary of two rooms and it enhanced the mixing efficiency. Number ratio of white particles was evaluated to investigate the mixing state or exchange rate between the rooms. The number ratio of white particles is given by dividing number of the white particles (N_w) by number of white and black particles (N_w+N_b) in left room. If the value of number ratio of white particles became 0.5,

equivalent amount of white and black particles were located in the left room. Figure 23 illustrates transient change in number ratio of white particles at the left room. These results indicate that the number ratio got closer to 0.5 as time elapsed. When the number of calculated particles was 200,000, number ratio of white particles was closest to 0.5. The results show that number ratio of white particles highly correlated with degree of mixing in this system. Hence, the total amount of powder is the most important factor affecting the degree of mixing in a twin-screw kneader. Much better mixing efficiency could be estimated if the powder bed height is gradually changed from the half height by trial and error.

The particle location was examined when the rotational speed was 60 rpm. Figure 24 illustrates the front and side views of the particle spatial location in the kneader. The particle spatial location at 8th and 16th rotation is shown in this figure. Even though the mixing was progressed, the particle location was hardly influenced in the depth direction. Horizontal movement of the particles becomes more active than vertical one in this system.

6. Conclusions

This study applied the DEM employing the SDF-based wall boundary model to

a twin-screw kneader as an example of an industrial system. First, the adequacy of the modeling was demonstrated in validation tests. In the validation tests, simulation and experimental results agreed well in terms of the spatial distribution of solid particles. Additionally, the particle flow tendencies agreed qualitatively in the simulation and experimental results. Consequently, the DEM employing the SDF boundary model was validated, and effects of operational conditions such as the amount of powder and rotational speed on the degree of mixing in a twin-screw kneader were thus investigated using the developed methodology.

The numerical simulation clarified the mixing mechanism behind observed phenomena. The mixing efficiency was affected by the amount of powder rather than the rotational speed. In particular, the amount of powder was shown to be of great importance to the twin-screw kneader. This is because the amount of powder affects the exchange of powder between the two rooms in the twin-screw system. When the vessel was filled with powder to around half height, the avalanches occurred near the boundary of two rooms and it enhanced the mixing efficiency. Consequently, the mixing efficiency was shown to increase when the exchange ratio increased in the two rooms in the twin-screw kneader.

When mixture of different particle sizes and/or different particle densities was

treated, mixing efficiency might change drastically because of the segregation. Application of the numerical technologies is also promising approach to investigate operational conditions and/or improvement of the blender design in the poly-dispersed systems for better mixing.

Acknowledgements

The authors express their sincere gratitude to Kurimoto, Ltd. and the Japan Society for the Promotion of Science for their financial support. The authors would like to thank Tazuko Ichinose for preparation of figures and tables.

References

[1] M.J. Rhodes, Introduction to Particle Technology, 2nd Edition, Wiley, 2008.

[2] A. Eitzlmayr, G. Koscher, G. Reynolds, Z. Huang, J. Booth, P. Shering, et al., Mechanistic Modeling of Modular Co-Rotating Twin-Screw Extruders, Int. J. Pharm. 474 (2014) 157–176.

[3] J. Bridgwater, Mixing of powders and granular materials by mechanical means—A perspective, Particuology. 10 (2012) 397–427.

[4] M. Alian, F. Ein-Mozaffari, S.R. Upreti, Analysis of the mixing of solid particles in a plowshare mixer via discrete element method (DEM), Powder Technol. 274 (2015) 77–87.

[5] A. Mehrotra, F.J. Muzzio, Comparing mixing performance of uniaxial and biaxial bin blenders, Powder Technol. 196 (2009) 1–7.

[6] P.A. Cundall, O.D.L. Strack, A discrete numerical model for granular assemblies, Geotechnique. 29 (1979) 47–65.

[7] M. Alian, F. Ein-Mozaffari, S.R. Upreti, J. Wu, Using discrete element method to analyze the mixing of the solid particles in a slant cone mixer, Chem. Eng. Res. Des. 93 (2014) 318–329.

[8] Y. Shigeto, M. Sakai, Parallel computing of discrete element method on multi-core processors, Particuology. 9 (2011) 398–405.

[9] S. Naik, R. Malla, M. Shaw, B. Chaudhuri, Investigation of comminution in a Wiley Mill: Experiments and DEM simulations, Powder Technol. 237 (2013) 338–354.

[10] D. Nguyen, A. Rasmuson, K. Thalberg, I.N. Björn, Numerical modelling of breakage and adhesion of loose fine-particle agglomerates, Chem. Eng. Sci. 116 (2014) 91–98.

[11] O.O. Olaofe, A. V. Patil, N.G. Deen, M.A. van der Hoef, J.A.M. Kuipers, Simulation of particle mixing and segregation in bidisperse gas fluidized beds, Chem. Eng. Sci. 108 (2014) 258–269.

[12] Y. Guo, C. Wassgren, B. Hancock, W. Ketterhagen, J. Curtis, Granular shear flows of flat disks and elongated rods without and with friction, Phys. Fluids. 25 (2013).

[13] Y. Guo, J.S. Curtis, Discrete element method simulations for complex granular flows, Annu. Rev. Fluid Mech. 47 (2015) 21–46.

[14] Y. Tsuji, T. Kawaguchi, T. Tanaka, Discrete particle simulation of two dimensional fluidized bed, Powder Technol. 77 (1993) 79–87.

[15] M. Sakai, Y. Yamada, Y. Shigeto, K. Shibata, V.M. Kawasaki, S. Koshizuka,

Large-scale discrete element modeling in a fluidized bed, Int. J. Numer. Meth. Fluids. 64 (2010) 1319–1335.

[16] M. Sakai, H. Takahashi, C.C. Pain, J.-P. Latham, J. Xiang, Study on a large-scale discrete element model for fine particles in a fluidized bed, Adv. Powder Technol. 23 (2012) 673–681.

[17] M. Sakai, M. Abe, Y. Shigeto, S. Mizutani, H. Takahashi, A. Viré, et al., Verification and validation of a coarse grain model of the DEM in a bubbling fluidized bed, Chem. Eng. J. 244 (2014) 33–43.

[18] J. Li, Approaching virtual process engineering with exploring mesoscience q, Chem. Eng. J. in press (n.d.).

[19] D. Jajcevic, E. Siegmann, C. Radeke, J.G. Khinast, Large-scale CFD-DEM simulations of fluidized granular systems, Chem. Eng. Sci. 98 (2013) 298–310.

[20] M. Sakai, S. Koshizuka, Large-scale discrete element modeling in pneumatic conveying, Chem. Eng. Sci. 64 (2009) 533–539.

[21] E.W.C. Lim, Y. Zhang, C.H. Wang, Effects of an electrostatic field in pneumatic conveying of granular materials through inclined and vertical pipes, Chem. Eng. Sci. 61 (2006) 7889–7908.

[22] J.J. Monaghan, An introduction to SPH, Comput. Phys. Comm. 48 (1988) 89–96.

[23] S. Koshizuka, A. Nobe, Y. Oka, Moving-particle semi-implicit method for fragmentation of incompressible fluid, Nucl. Sci. Eng. 123 (1996) 421–434.

[24] M. Sakai, Y. Shigeto, X. Sun, T. Aoki, T. Saito, J. Xiong, et al., Lagrangian–Lagrangian modeling for a solid–liquid flow in a cylindrical tank, Chem. Eng. J. 200-202 (2012) 663–672.

[25] X. Sun, M. Sakai, M.-T. Sakai, Y. Yamada, A Lagrangian–Lagrangian coupled method for three-dimensional solid–liquid flows involving free surfaces in a rotating cylindrical tank, Chem. Eng. J. 246 (2014) 122–141.

[26] Y. Yamada, M. Sakai, Lagrangian–Lagrangian simulations of solid–liquid flows in a bead mill, Powder Technol. 239 (2013) 105–114.

[27] X. Sun, M. Sakai, Y. Yamada, Three-dimensional simulation of a solid–liquid flow by the DEM–SPH method, J. Comput. Phys. 248 (2013) 147–176.

[28] Z.Y. Zhou, S.B. Kuang, K.W. Chu, A.B. Yu, Discrete particle simulation of particle–fluid flow: model formulations and their applicability, J. Fluid Mech. 661 (2010) 482–510.

[29] D. Barrasso, T. Eppinger, F.E. Pereira, R. Aglave, K. Debus, S.K. Bermingham, et al., A multi-scale , mechanistic model of a wet granulation process using a novel bi-directional PBM – DEM coupling algorithm, Chem. Eng. Sci. 123

(2015) 500–513.

[30] Y. Shigeto, M. Sakai, Arbitrary-shaped wall boundary modeling based on signed distance functions for granular flow simulations, Chem. Eng. J. 231 (2013) 464–476.

[31] R.M. Dhenge, K. Washino, J.J. Cartwright, M.J. Hounslow, A.D. Salman, Twin screw granulation using conveying screws: Effects of viscosity of granulation liquids and flow of powders, Powder Technol. 238 (2013) 77–90.

[32] B. Mu, M.R. Thompson, Examining the mechanics of granulation with a hot melt binder in a twin-screw extruder, Chem. Eng. Sci. 81 (2012) 46–56.

[33] A. Kumar, J. Vercruysse, V. Vanhoorne, M. Toiviainen, P.-E. Panouillot, M. Juuti, et al., Conceptual framework for model-based analysis of residence time distribution in twin-screw granulation, Eur. J. Pharm. Sci. 71 (2015) 25–34.

[34] J. Vercruysse, A. Burggraeve, M. Fonteyne, P. Cappuyns, U. Delaet, I. Van Assche, et al., Impact of screw configuration on the particle size distribution of granules produced by twin screw granulation, Int. J. Pharm. 479 (2015) 171–180.

[35] P.M.C. Lacey, Developments in the theory of particle mixing, J. Appl. Chem. 4 (1954) 257–268.

[36] S. Adam, D. Suzzi, C. Radeke, J.G. Khinast, An integrated Quality by Design (QbD) approach towards design space definition of a blending unit operation by Discrete Element Method (DEM) simulation., Eur. J. Pharm. Sci. 42 (2011) 106–15.

[37] M. Halidan, G.R. Chandratilleke, S.L.I. Chan, A.B. Yu, J. Bridgwater, Prediction of the mixing behaviour of binary mixtures of particles in a bladed mixer, Chem. Eng. Sci. 120 (2014) 37–48.

Nomenclature

m	:	particle mass (kg)
$\boldsymbol{v}$	:	particle velocity (m/s)
$\boldsymbol{F}_C$	:	contact force (N)
$\boldsymbol{F}_g$	:	gravitational force (N)
$\boldsymbol{T}$	:	torque (N m)
I	:	moment of inertia (kg m^2)
k	:	spring constant (N/m)
e	:	coefficient of restitution (-)
$\boldsymbol{n}$	:	normal vector (-)
$\boldsymbol{t}$	:	tangential vector (-)
d	:	minimal distance (m)
s	:	sign (-)
$\boldsymbol{x}$	:	position vector (m)
$\boldsymbol{F}$	:	elastic force (N)
P	:	potential energy (J)
p	:	total number of sampling cells from this system (-)
c_i	:	local concentration in sampling cells (-)
c_m	:	overall proportion of one type of particle in the system (-)
q	:	average particle number over all sampling cells (-)
N	:	number of particles (-)
N_w	:	number of white particles (-)
N_b	:	number of black particles (-)

Greek letters

$\boldsymbol{\omega}$	:	angular velocity (rad/s)
$\boldsymbol{\delta}$	:	displacement (m)
η	:	damping coefficient (-)
μ	:	coefficient of friction (-)
ϕ	:	signed distance function (m)
σ_t^2	:	variance based on the current particle location (-)
σ_0^2	:	variance in a completely segregated system (-)
σ_r^2	:	variance in a perfectly mixed system (-)
Ω	:	rotational speed of a paddle (rad/s)

Subscripts

n : normal component

t : tangential component

Superscript

SDF : signed distance function

Table 1 Physical properties in the validation test

Item	Unit	Value
Diameter	mm	1.0
Density	kg/m^3	2500
Spring constant	N/m	1000
Coefficient of restitution	-	0.9
Coefficient of friction	-	0.3

Table 2 Conditions in the validation test

		Case 1-1	Case 1-2
Powder weight	kg	0.262	0.524
Number of particles	-	200,000	400,000
Time step	s	$1.0x10^{-5}$	
Rotational speed	rpm	20	60

Table 3 Calculation conditions

	Number of particles N	Rotational speed Ω (rpm)	Time step (s)
Case 2-1	100,000	15	$1.0x10^{-5}$
Case 2-2		30	
Case 2-3		60	
Case 3-1	200,000	15	
Case 3-2		30	
Case 3-3		60	
Case 4-1	400,000	15	
Case 4-2		30	
Case 4-3		60	

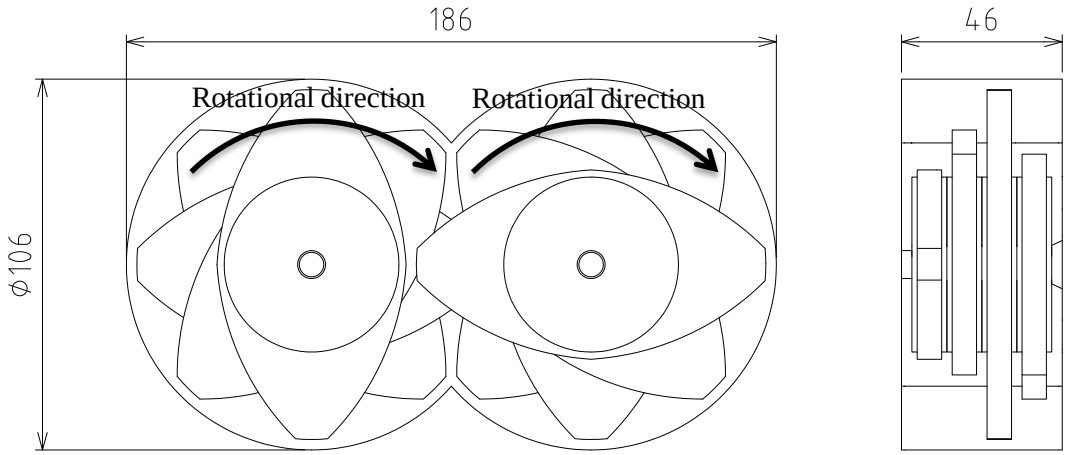

(a) Front view (b) Side view

Fig. 1 Schematic diagram of a twin-screw kneader

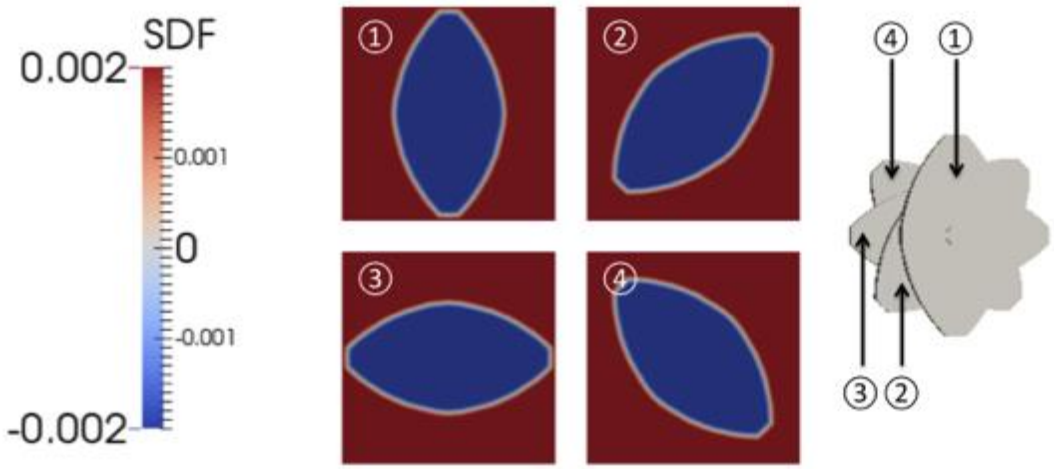

Fig. 2 Signed distance functions of a paddle

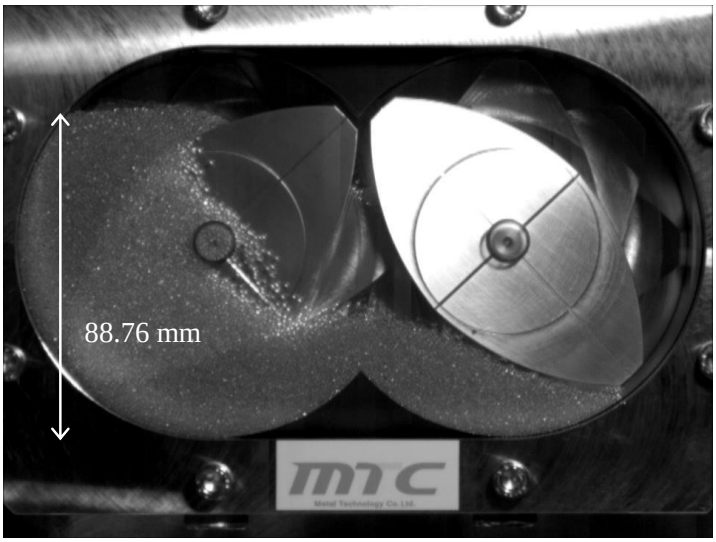

(a) Experiment

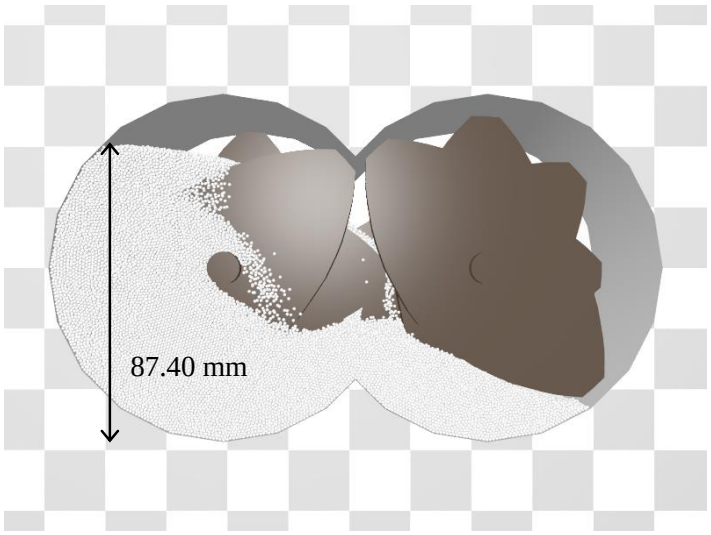

(b) Simulation

Fig. 3 Validation test results (Case 1-1)

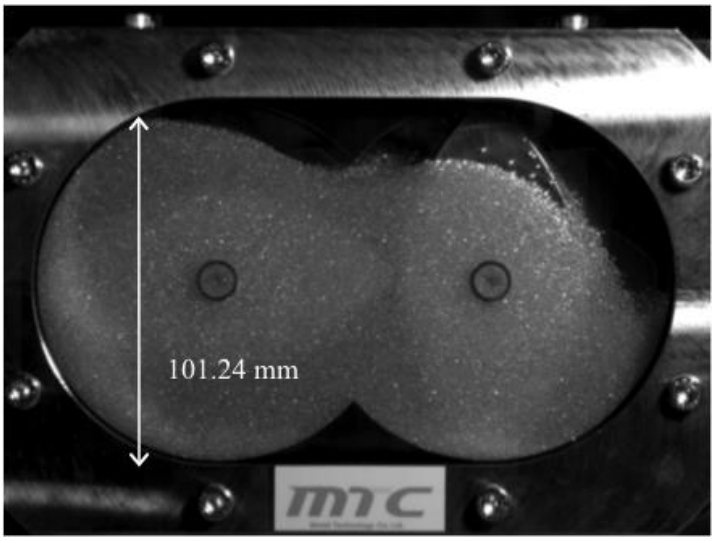

(a) Experiment

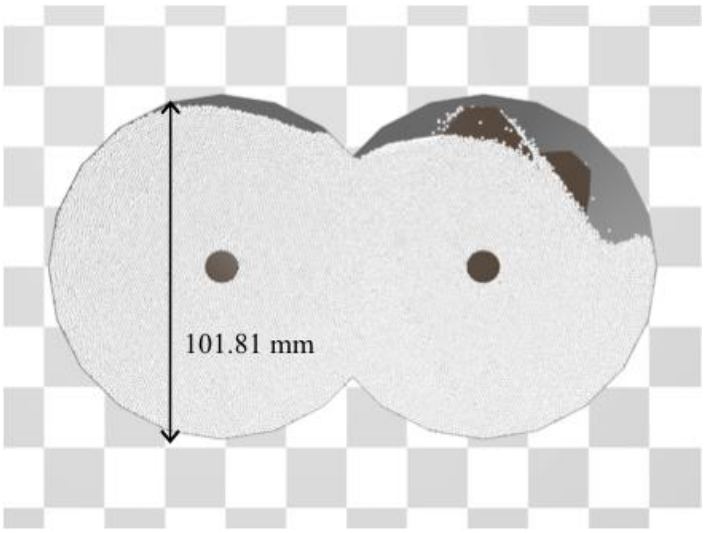

(b) Simulation

Fig. 4 Validation test results (Case 1-2)

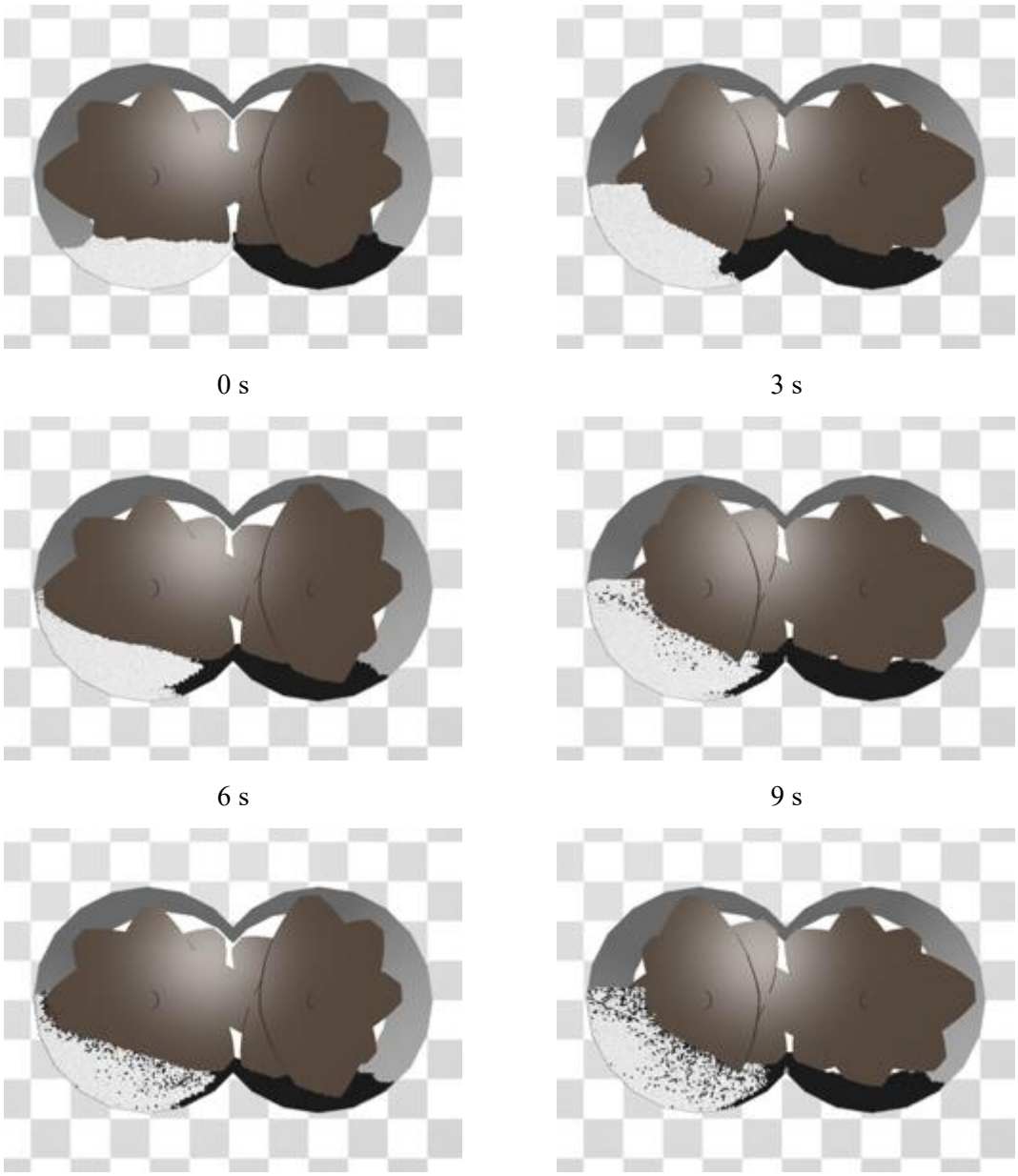

Fig. 5(a) Mixing state in Case 2-1 (N = 100,000, Ω = 15 rpm)

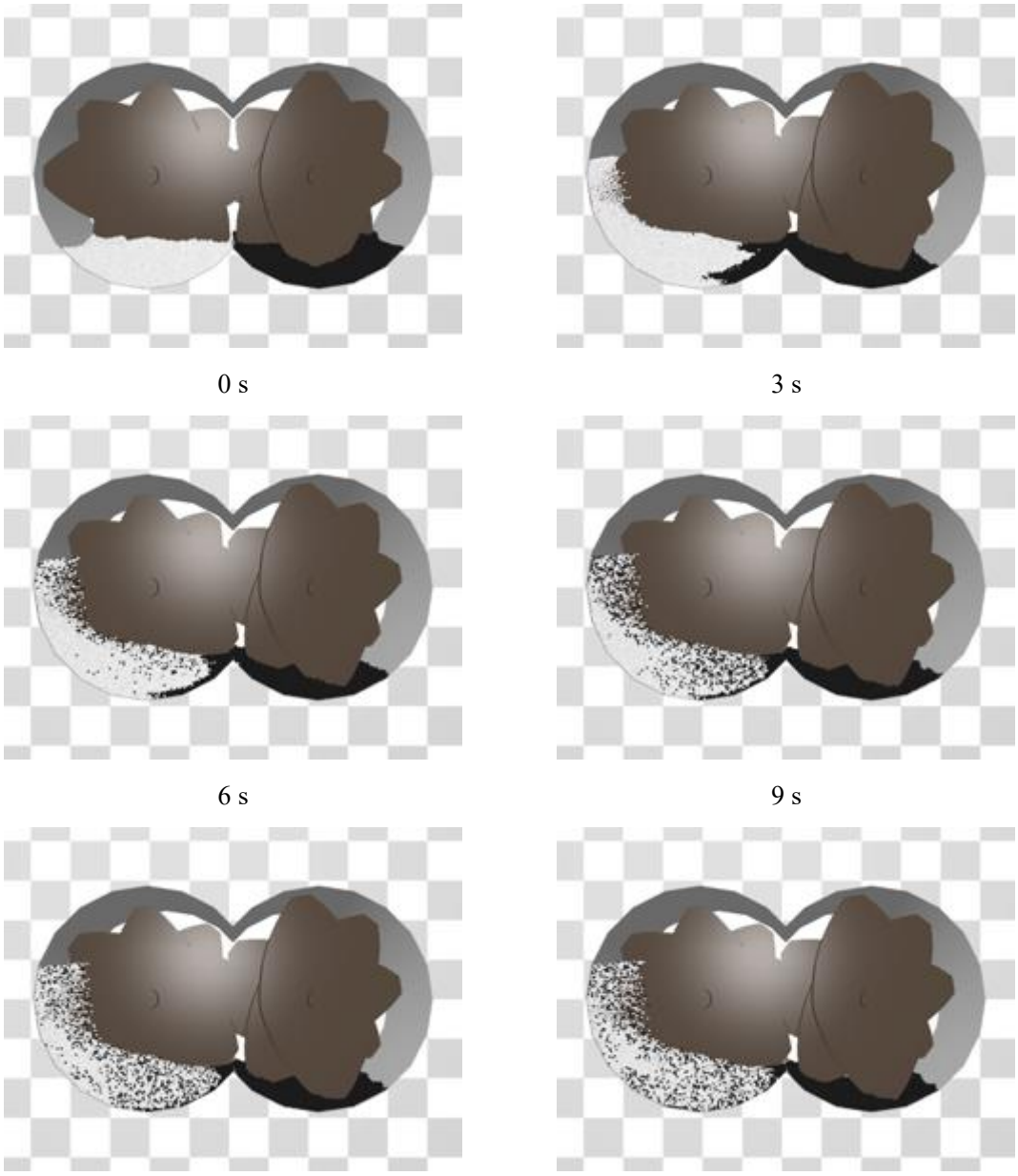

Fig. 5(b) Mixing state in Case 2-2 (N = 100,000, Ω = 30 rpm)

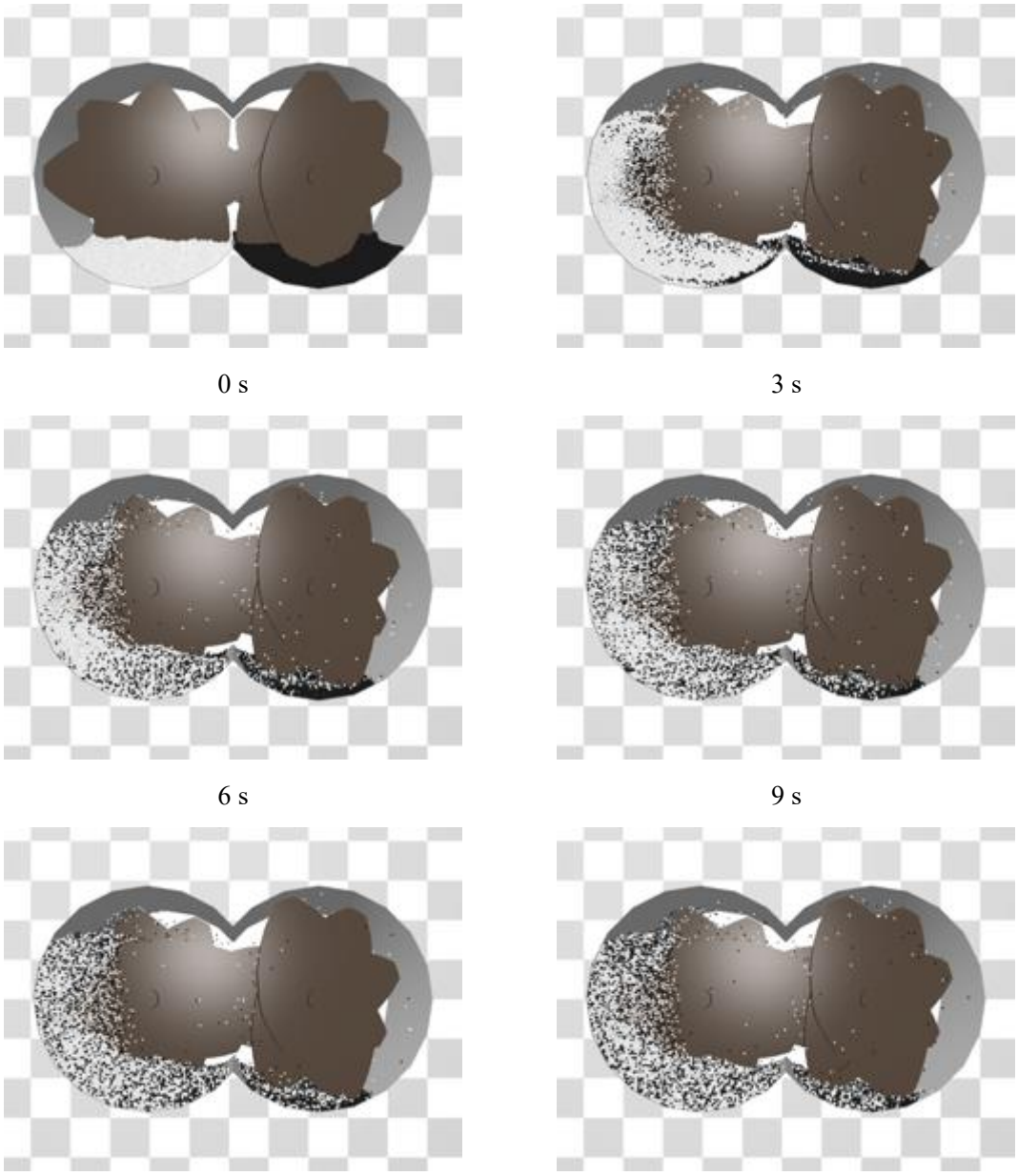

Fig. 5(c) Mixing state in Case 2-3 (N = 100,000, Ω = 60 rpm)

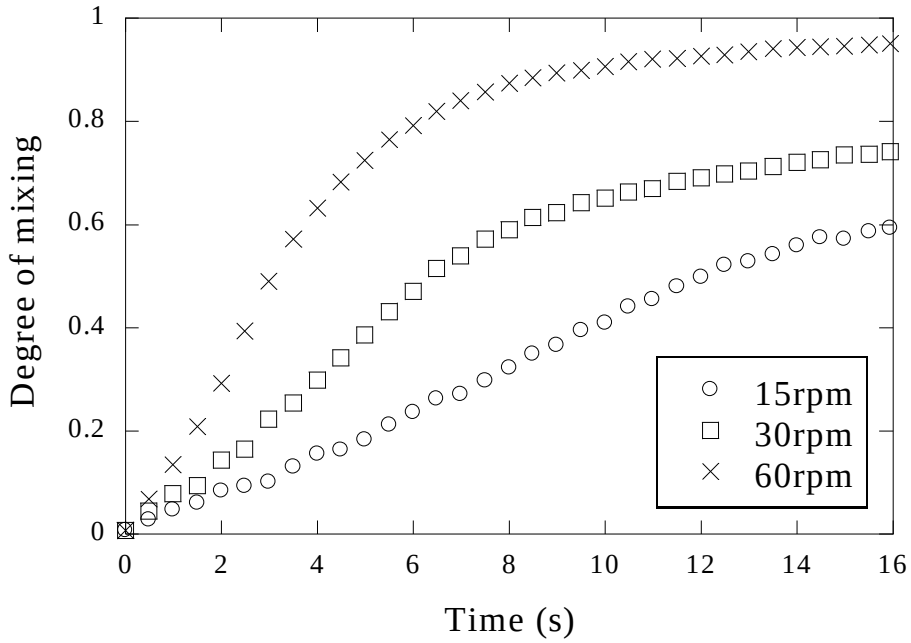

Fig. 6 Transient change in the degree of mixing at different rotational speeds (Case 2)

Second rotation

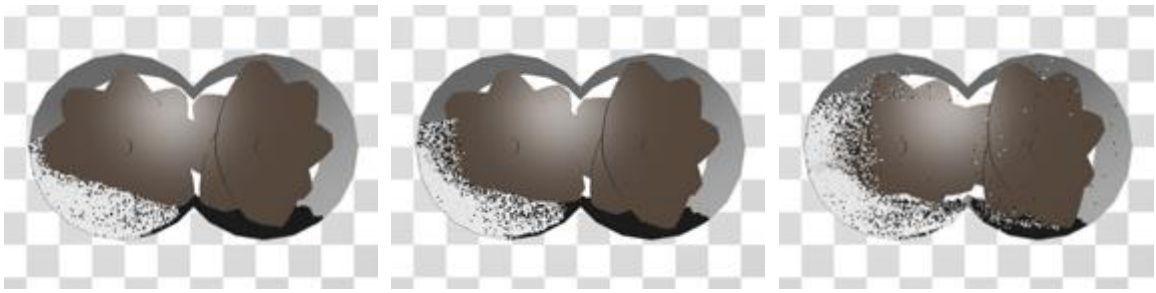

Fourth rotation

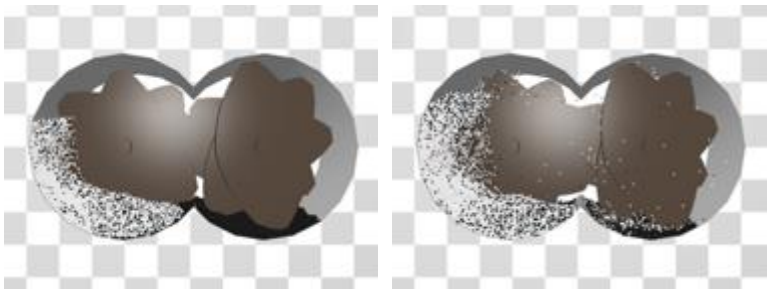

Sixth rotation

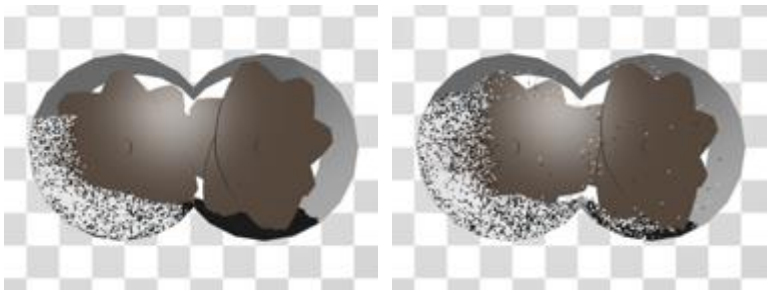

Eighth rotation

Case 2-1 (15 rpm) Case 2-2 (30 rpm) Case 2-3 (60 rpm)

Fig. 7 Representative snapshots of the degree of mixing per number of rotations (Case 2)

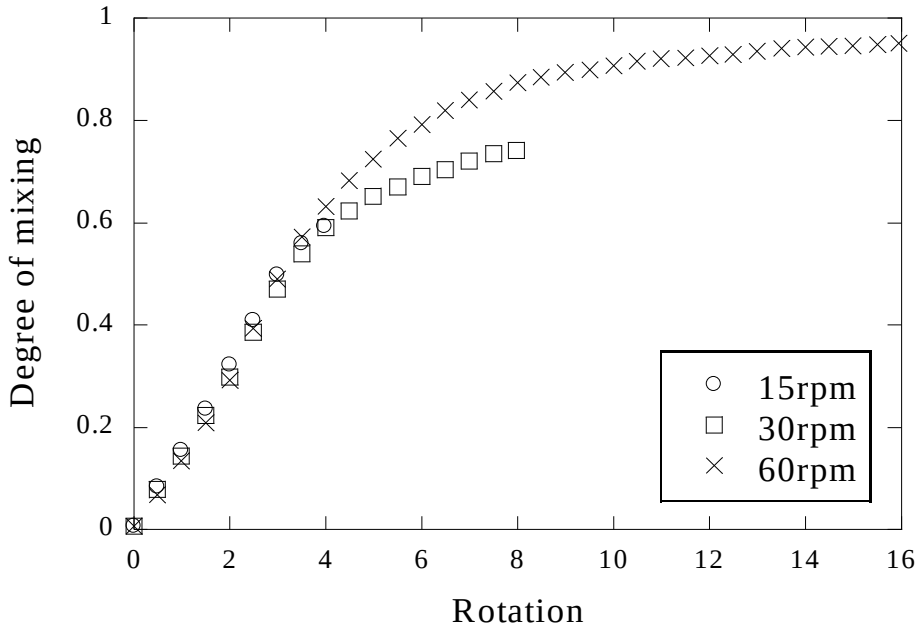

Fig. 8 Relation between the mixing index and rotational number (Case 2)

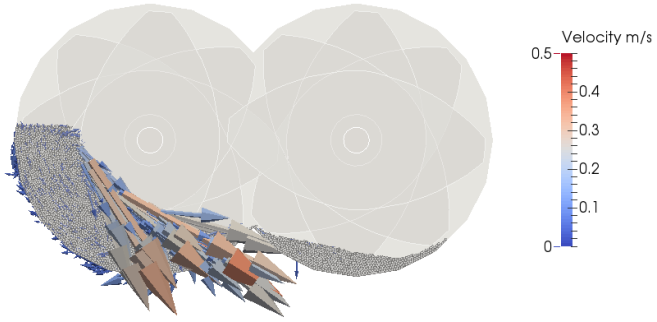

Ω = 15 rpm

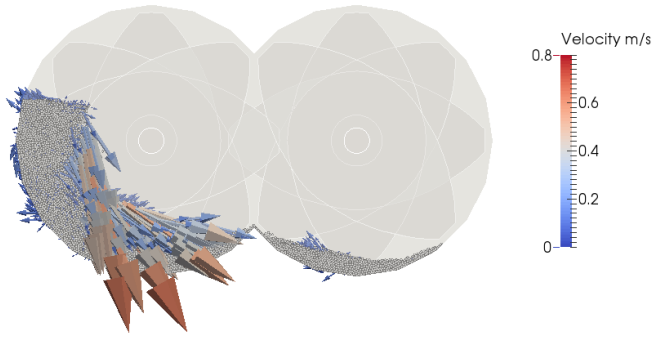

Ω = 30 rpm

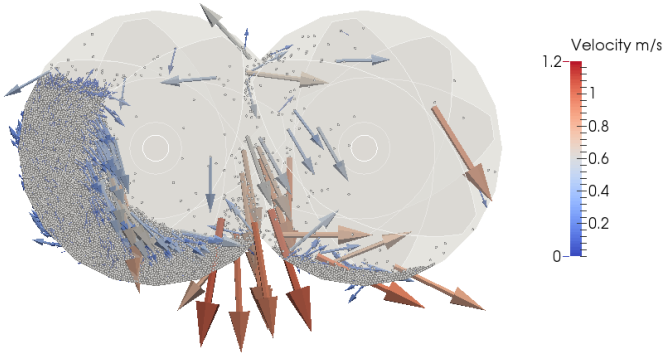

Ω = 60 rpm

Fig. 9 Velocity distribution of particles in the twin-screw kneader (N = 100,000)

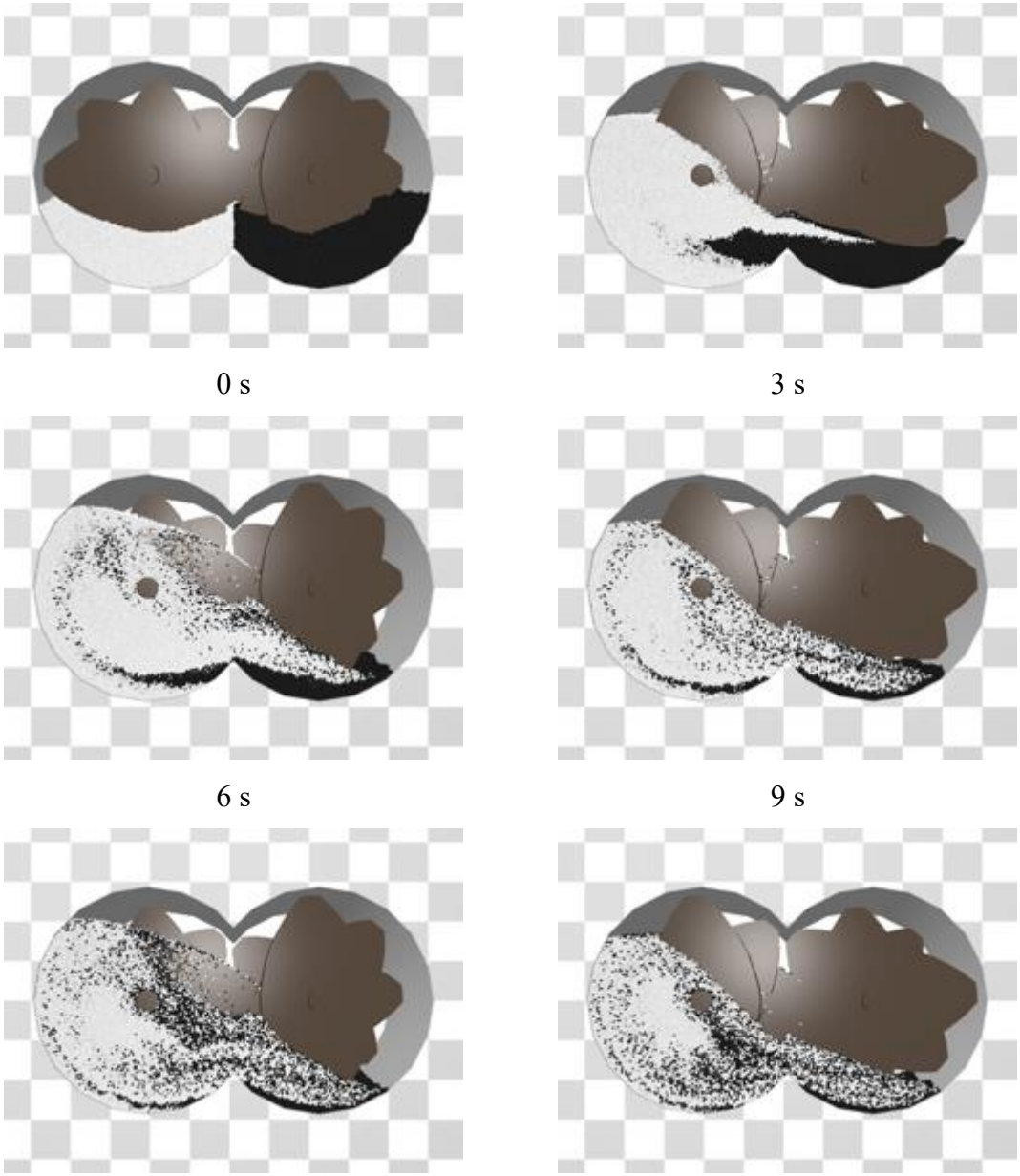

Fig. 10(a) Mixing state in Case 3-1 (N = 200,000, Ω = 15 rpm)

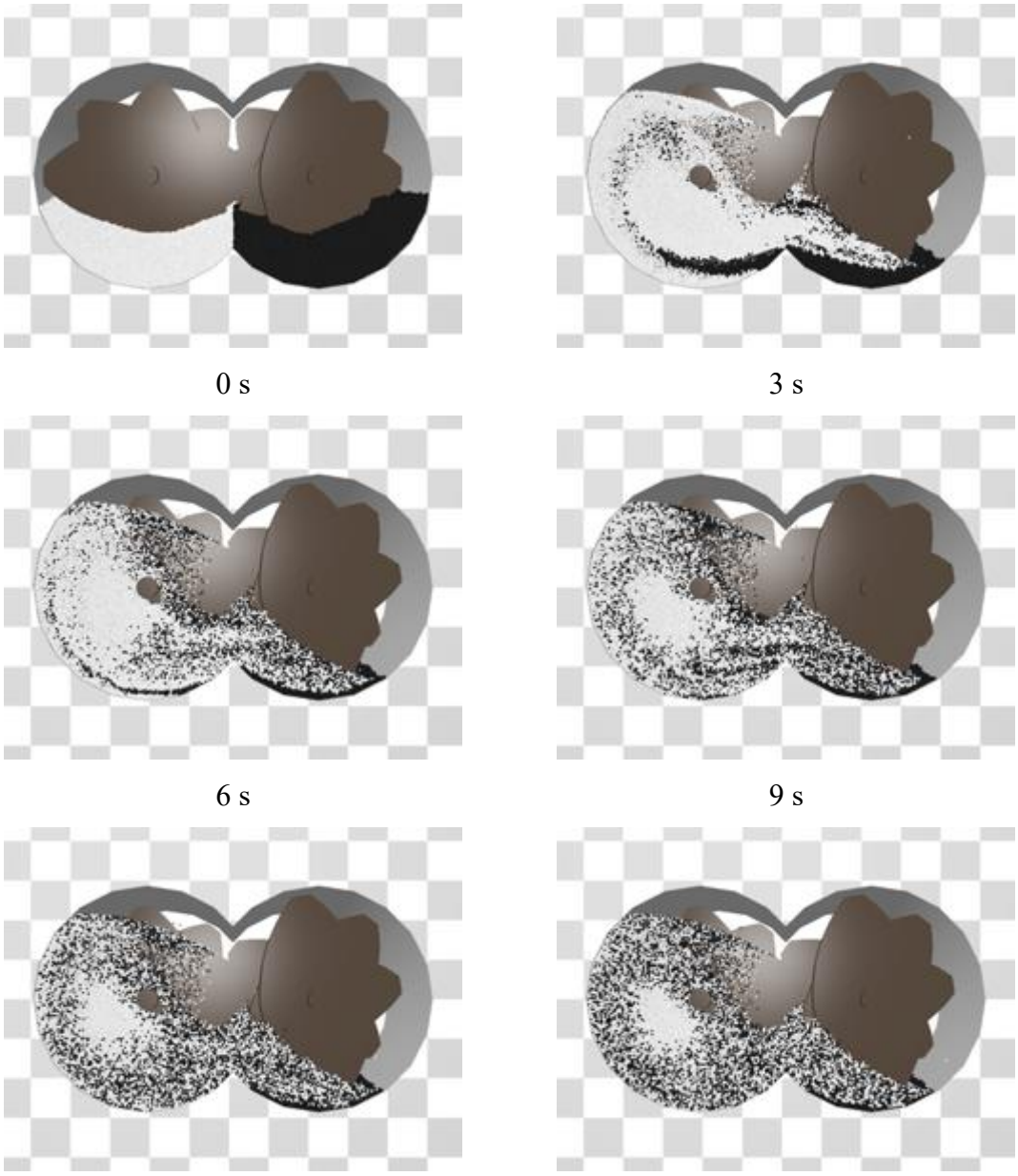

Fig. 10(b) Mixing state in Case 3-2 (N = 200,000, Ω = 30 rpm)

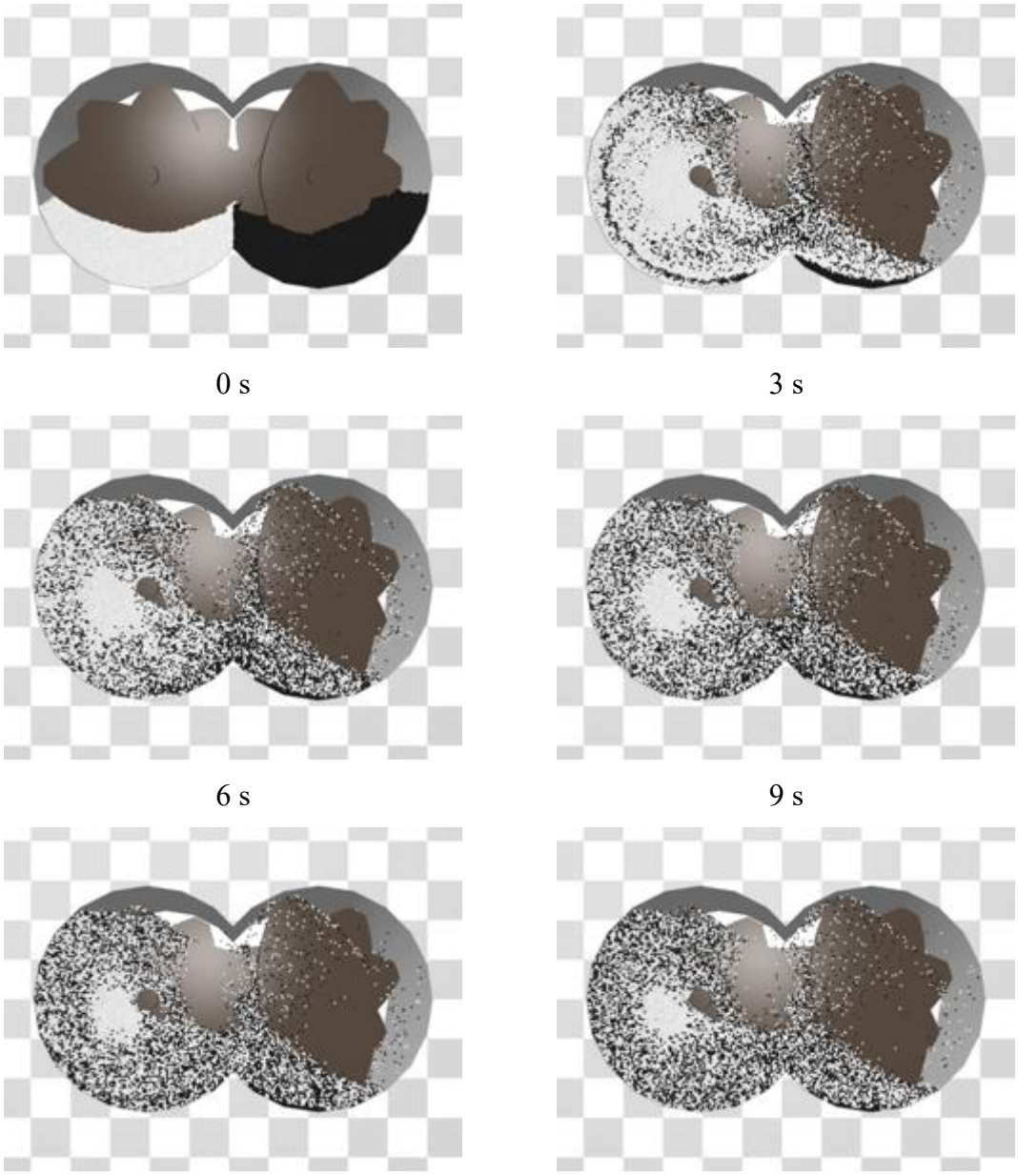

Fig. 10(c) Mixing state in Case 3-3 (N = 200,000, Ω = 60 rpm)

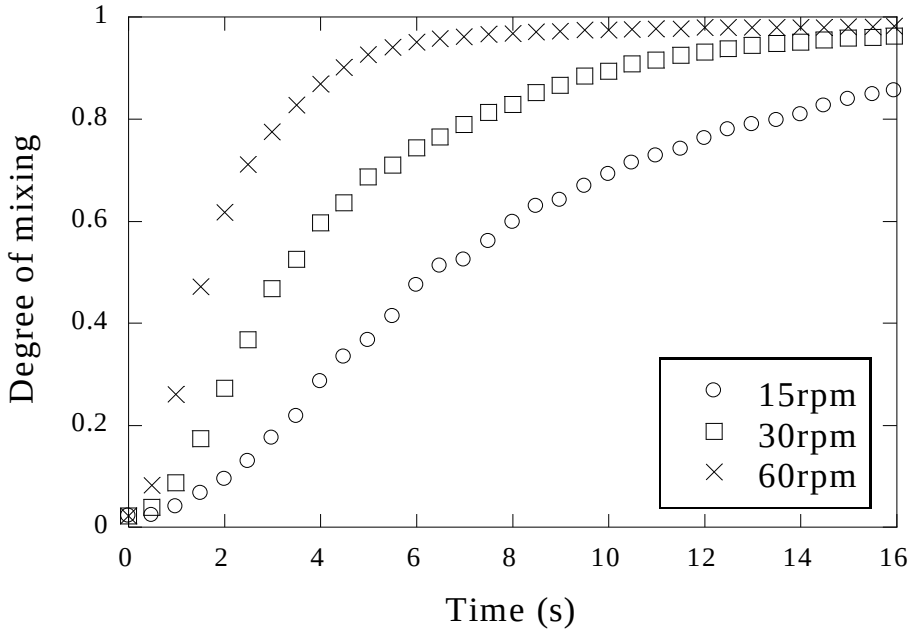

Fig. 11 Transient change in the degree of mixing at different rotational speeds (Case 3)

Second rotation

Fourth rotation

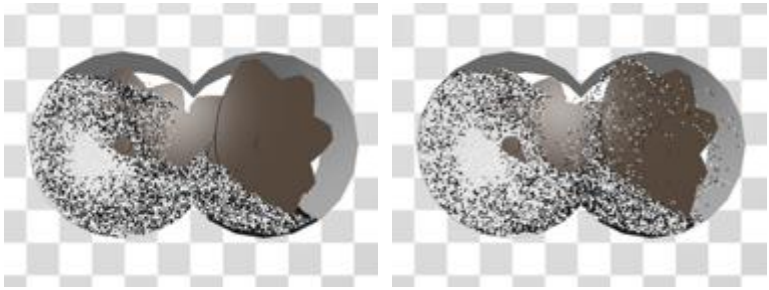

Sixth rotation

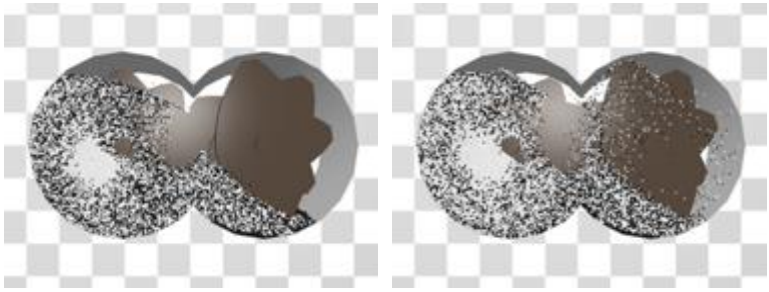

Eighth rotation

Case 3-1 (15 rpm) Case 3-2 (30 rpm) Case 3-3 (60 rpm)

Fig. 12 Representative snapshots of the degree of mixing per number of rotations (Case 3)

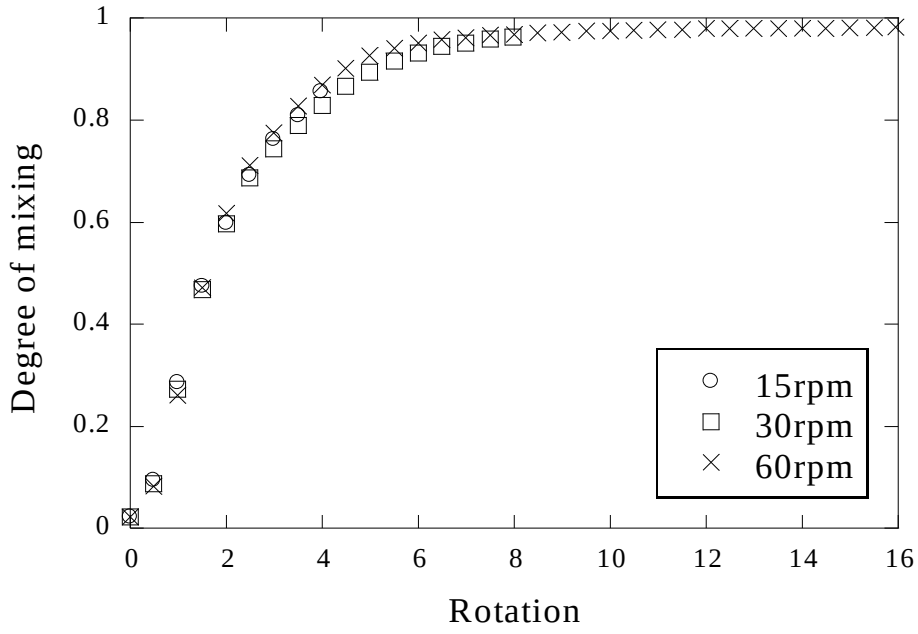

Fig. 13 Relation between the mixing index and rotational number (Case 3)

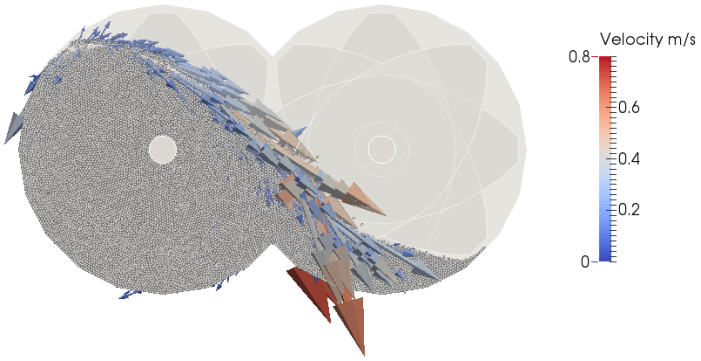

Ω = 15 rpm

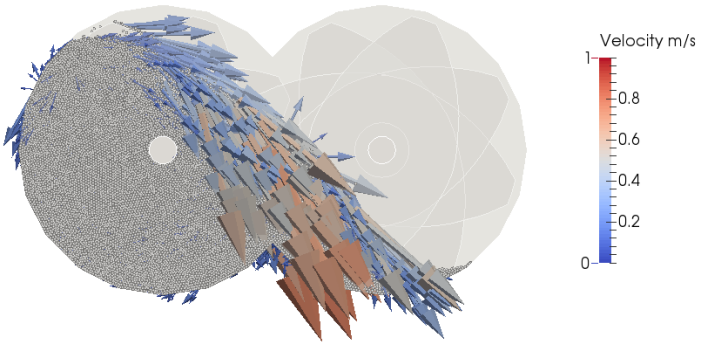

Ω = 30 rpm

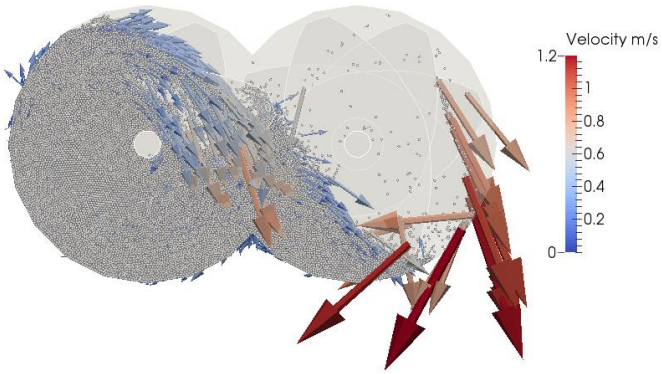

Ω = 60 rpm

Fig. 14 Velocity distribution of particles in the twin-screw kneader (N = 200,000)

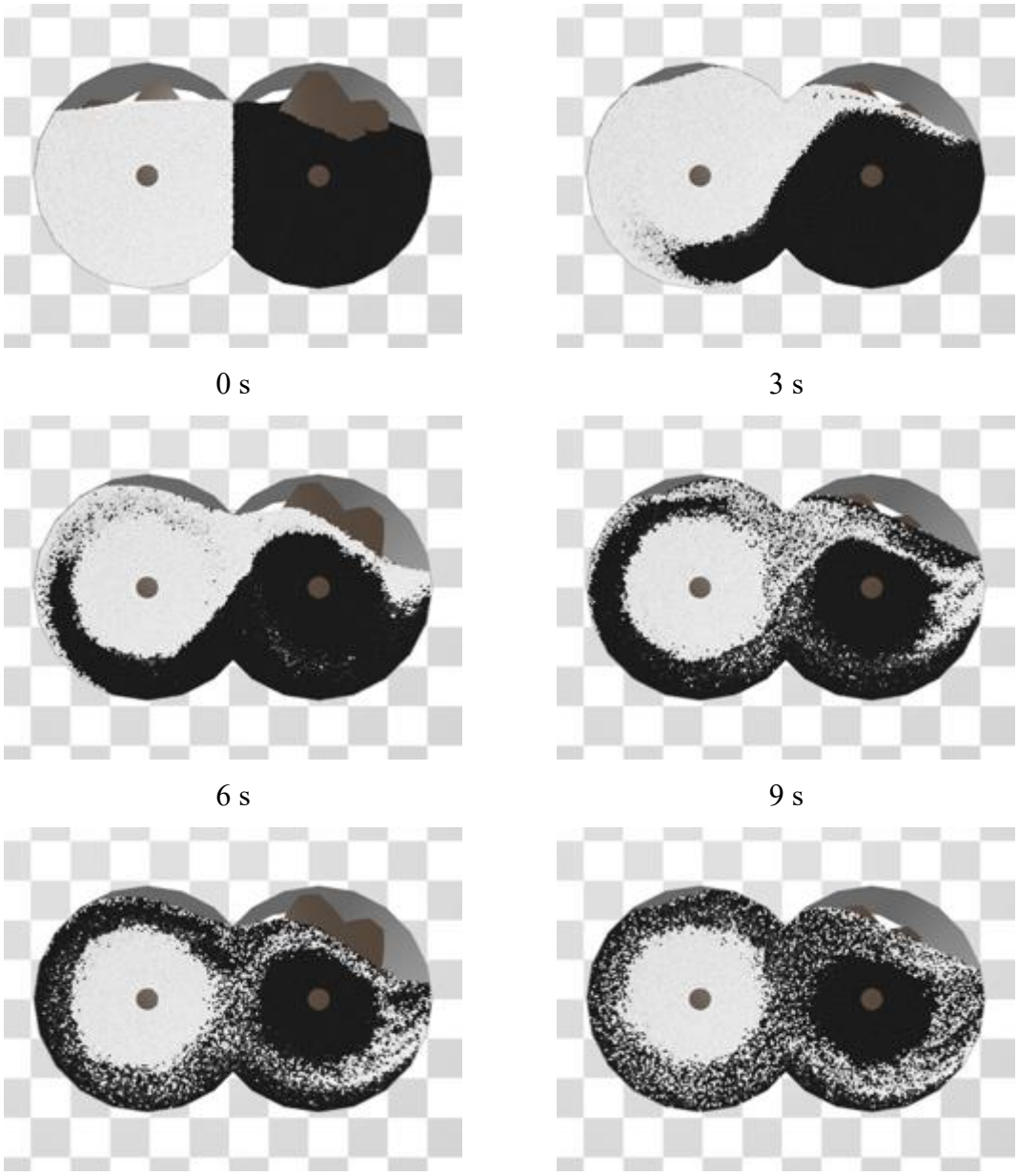

Fig. 15(a) Mixing state in Case 4-1 (N = 400,000, Ω = 15 rpm)

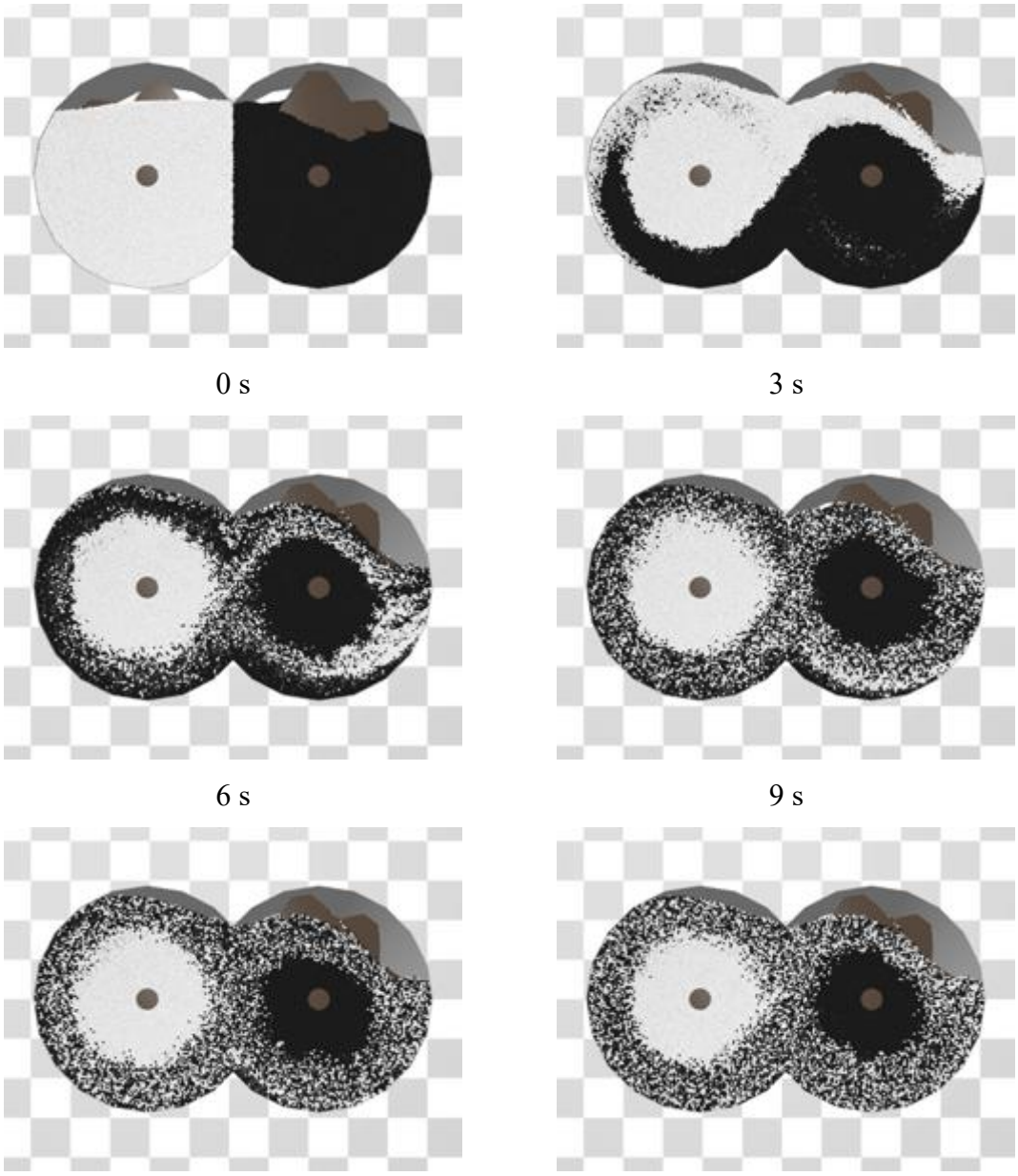

Fig. 15(b) Mixing state in Case 4-2 (N = 400,000, Ω = 30 rpm)

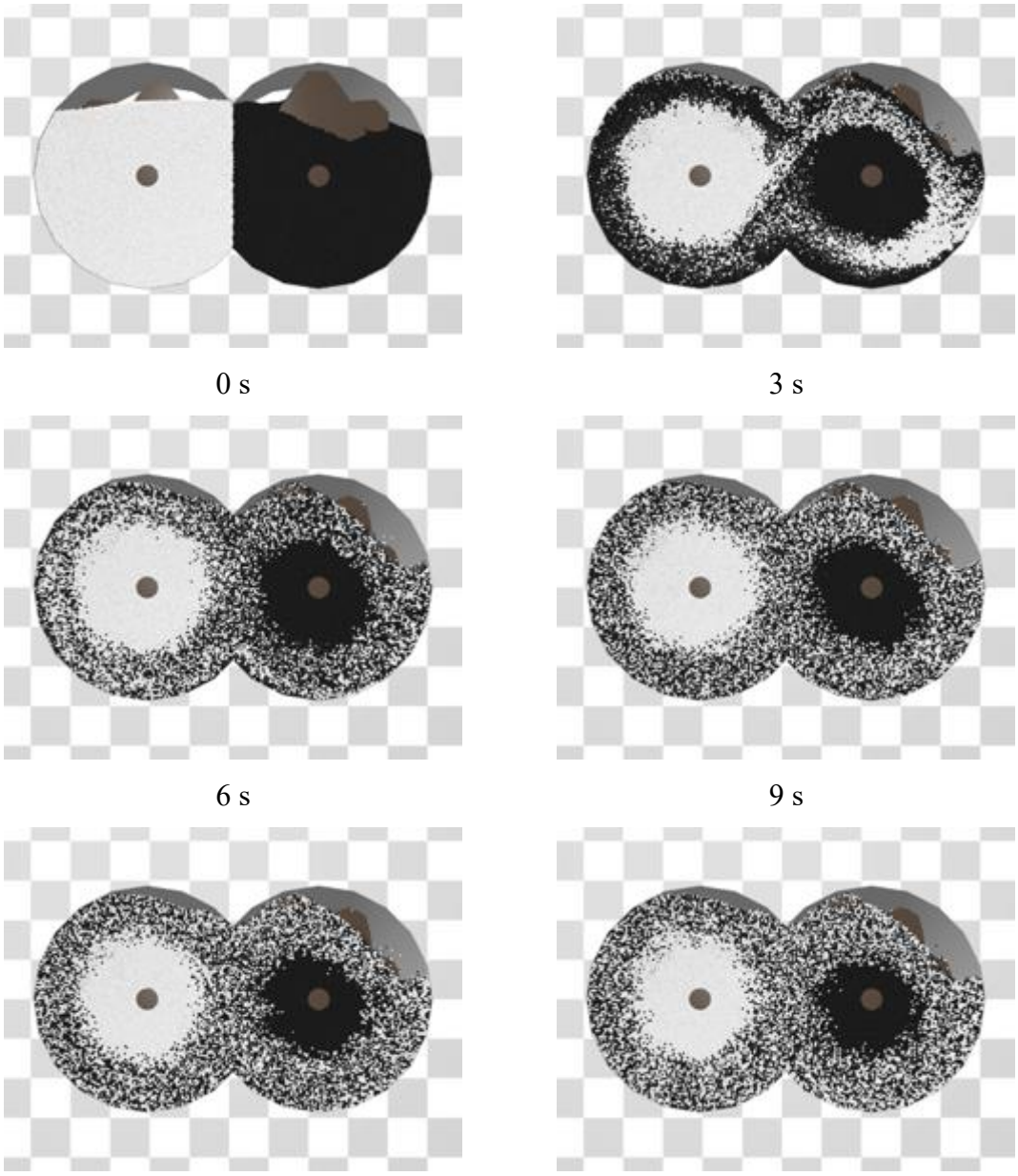

Fig. 15(c) Mixing state in Case 4-3 (N = 400,000, Ω = 60 rpm)

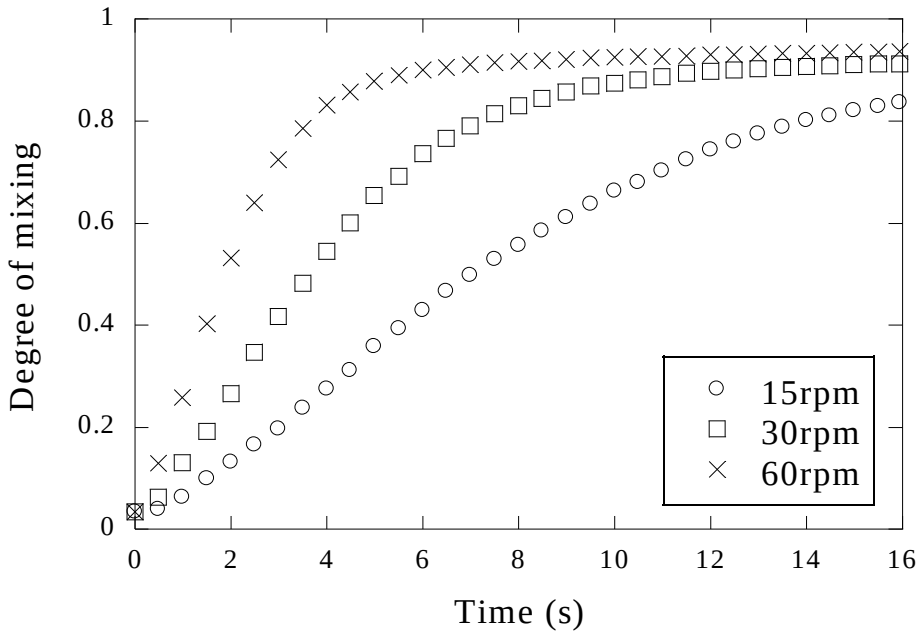

Fig. 16 Transient change in the degree of mixing at different rotational speeds (Case 4)

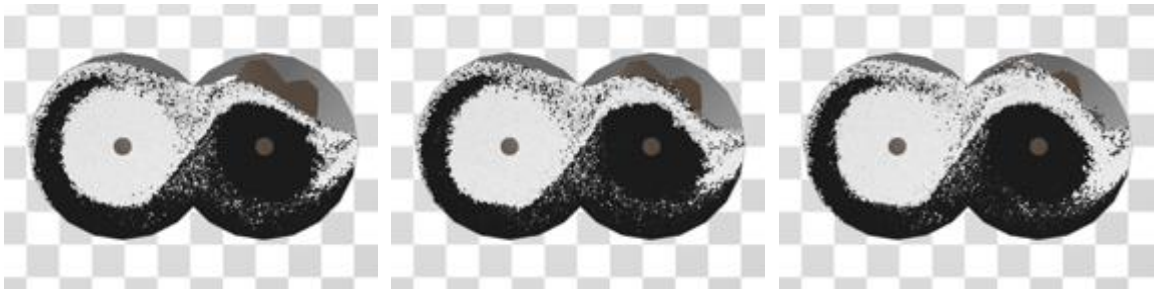

Second rotation

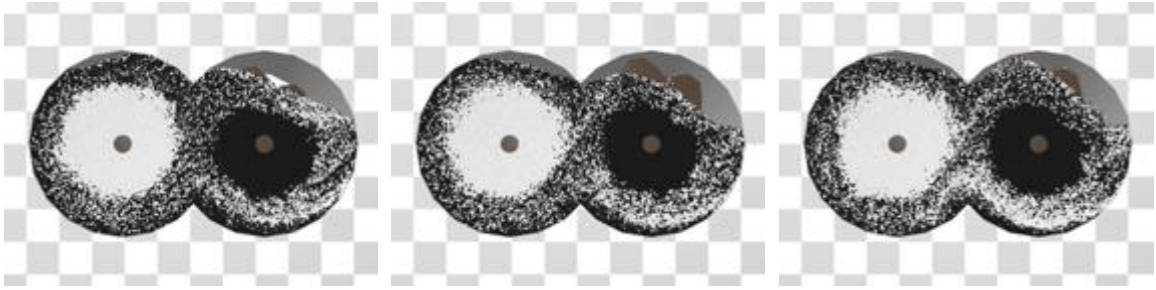

Fourth rotation

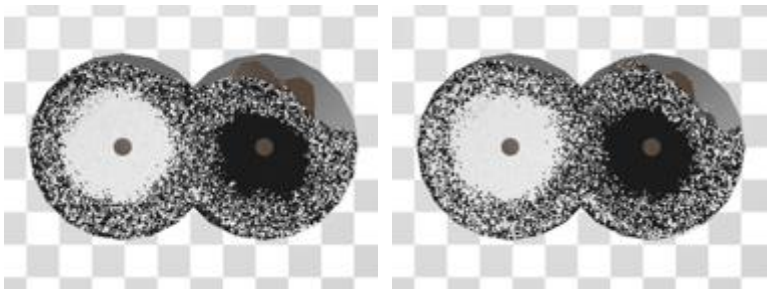

Sixth rotation

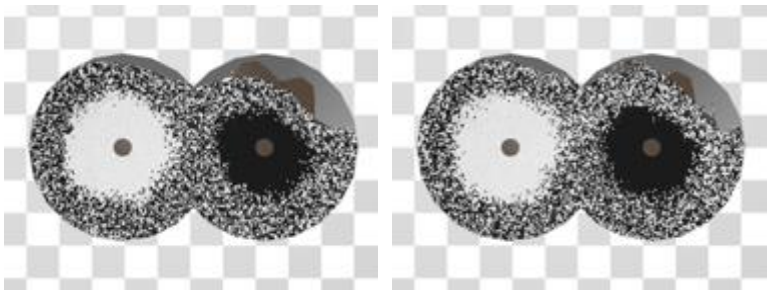

Eighth rotation

Case 4-1 (15 rpm) Case 4-2 (30 rpm) Case 4-3 (60 rpm)

Fig. 17 Representative snapshots of the degree of mixing per number of rotations (Case 4)

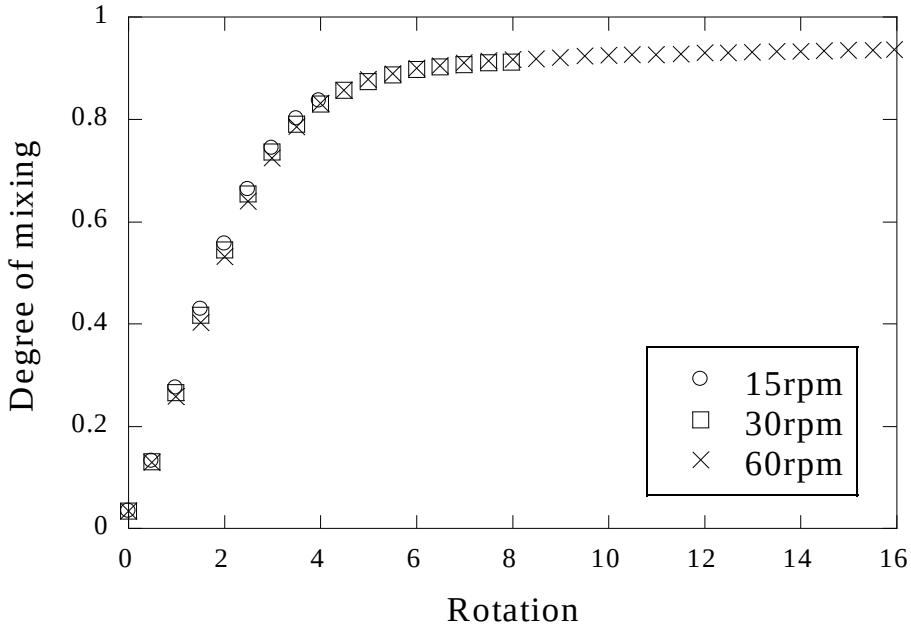

Fig. 18 Relation between the mixing index and rotational number (Case 4)

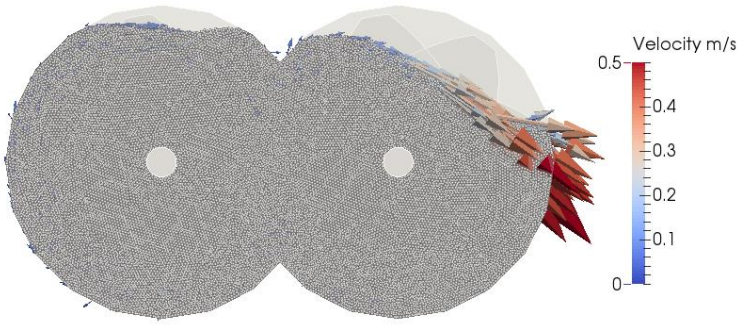

Ω = 15 rpm

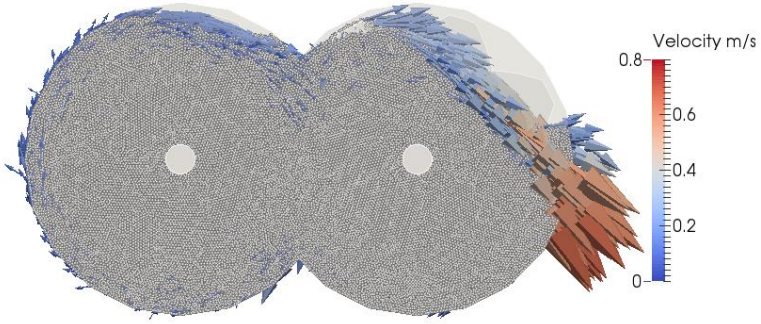

Ω = 30 rpm

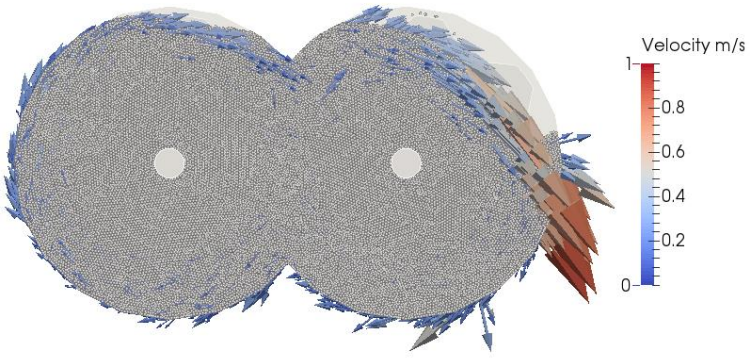

Ω = 60 rpm

Fig. 19 Velocity distribution of particles in the twin-screw kneader (N = 400,000)

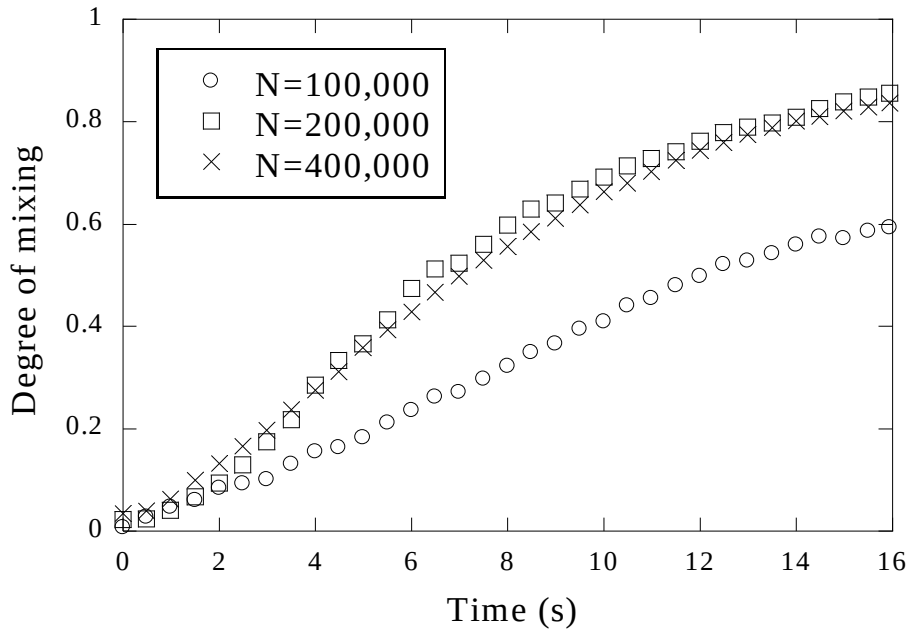

Fig. 20 Effect of the number of particles on the mixing degree at 15 rpm

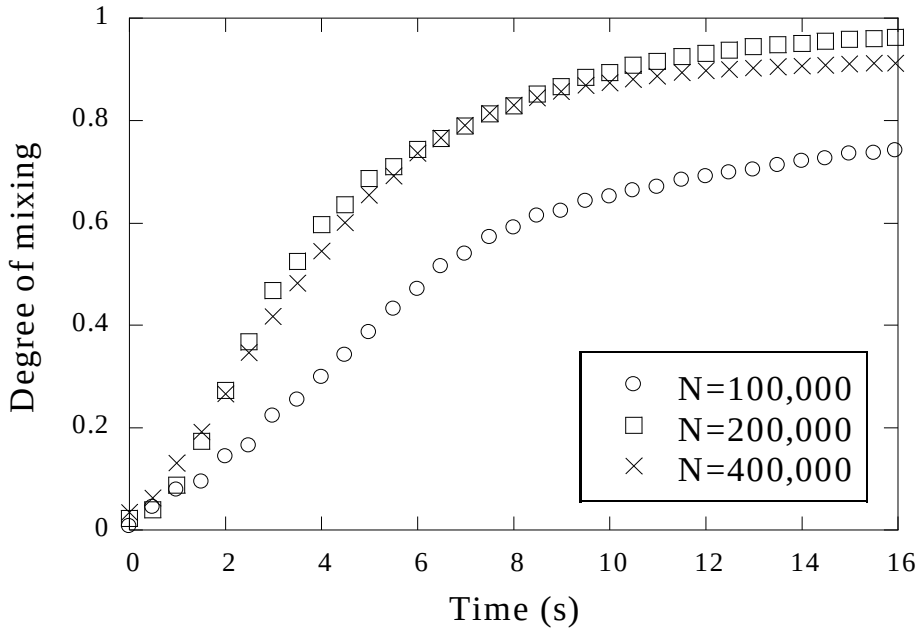

Fig. 21 Effect of the number of particles on the mixing degree at 30 rpm

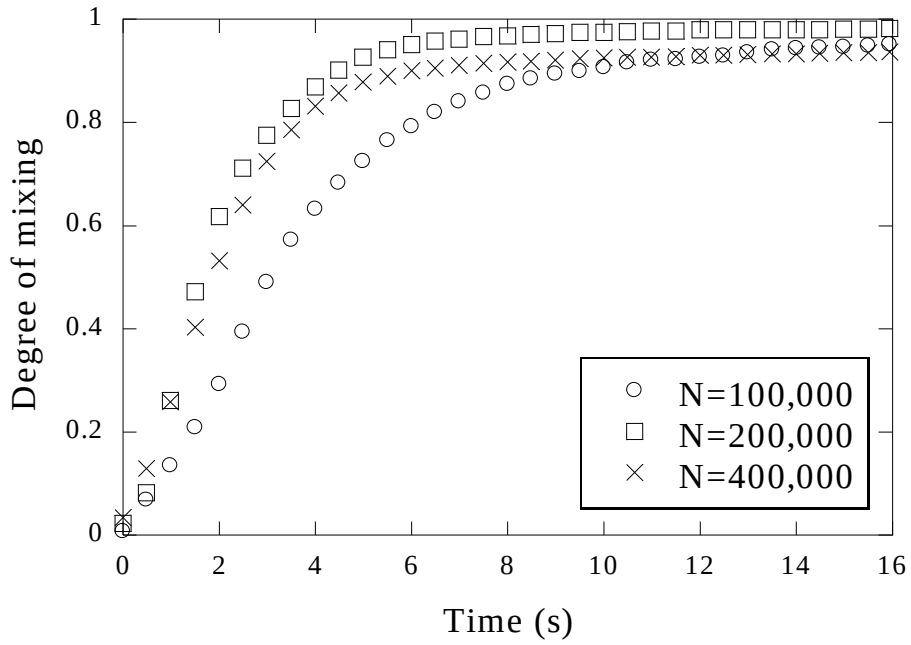

Fig. 22 Effect of the number of particles on the mixing degree at 60 rpm

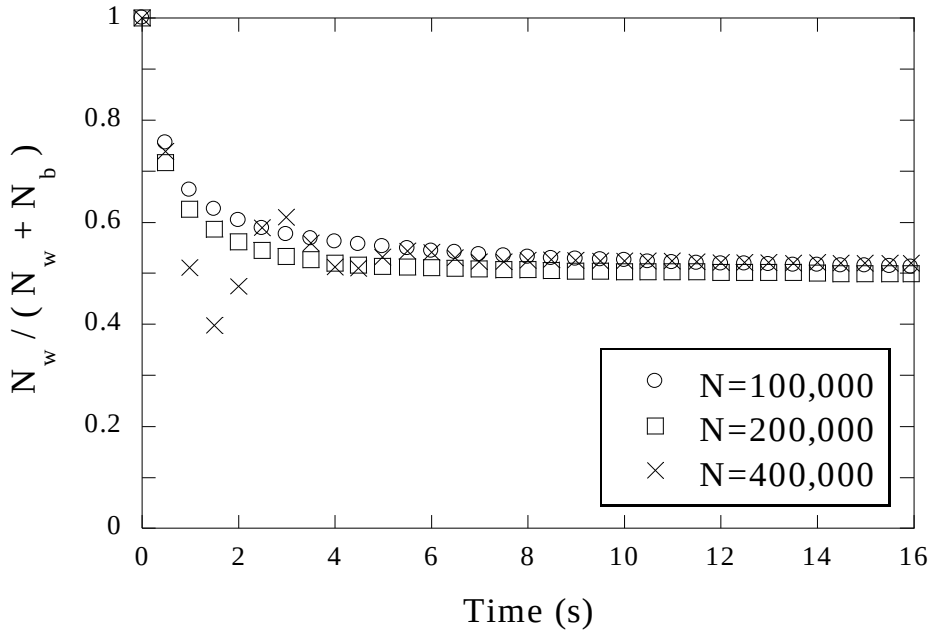

Fig. 23 Transient change in number ratio of white particles at the left room

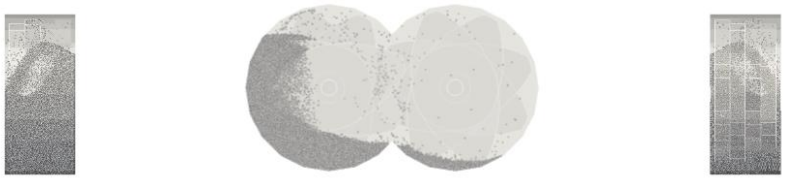

(a) 8th rotation

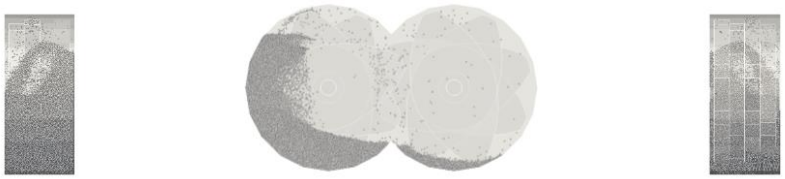

(b) 16th rotation

N=100,000

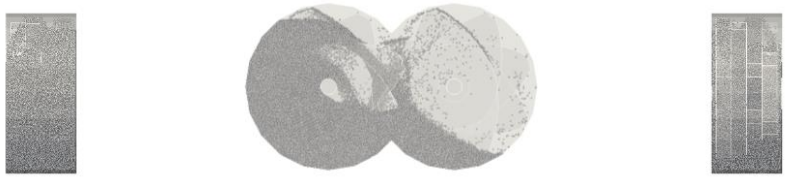

(a) 8th rotation

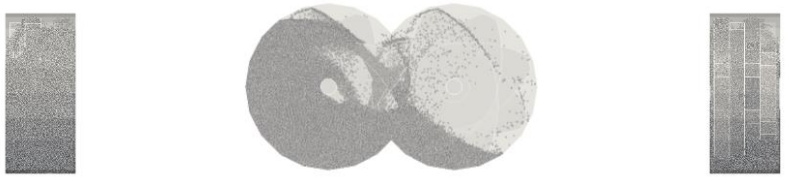

(b) 16th rotation

N=200,000

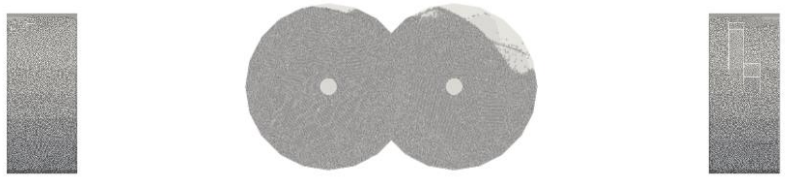

(a) 8th rotation

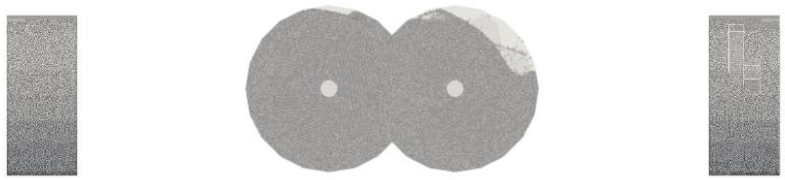

(b) 16th rotation

N=400,000

Left view Front view Right view

Fig. 24 Spatial location of particles in the blender (Ω = 60 rpm)